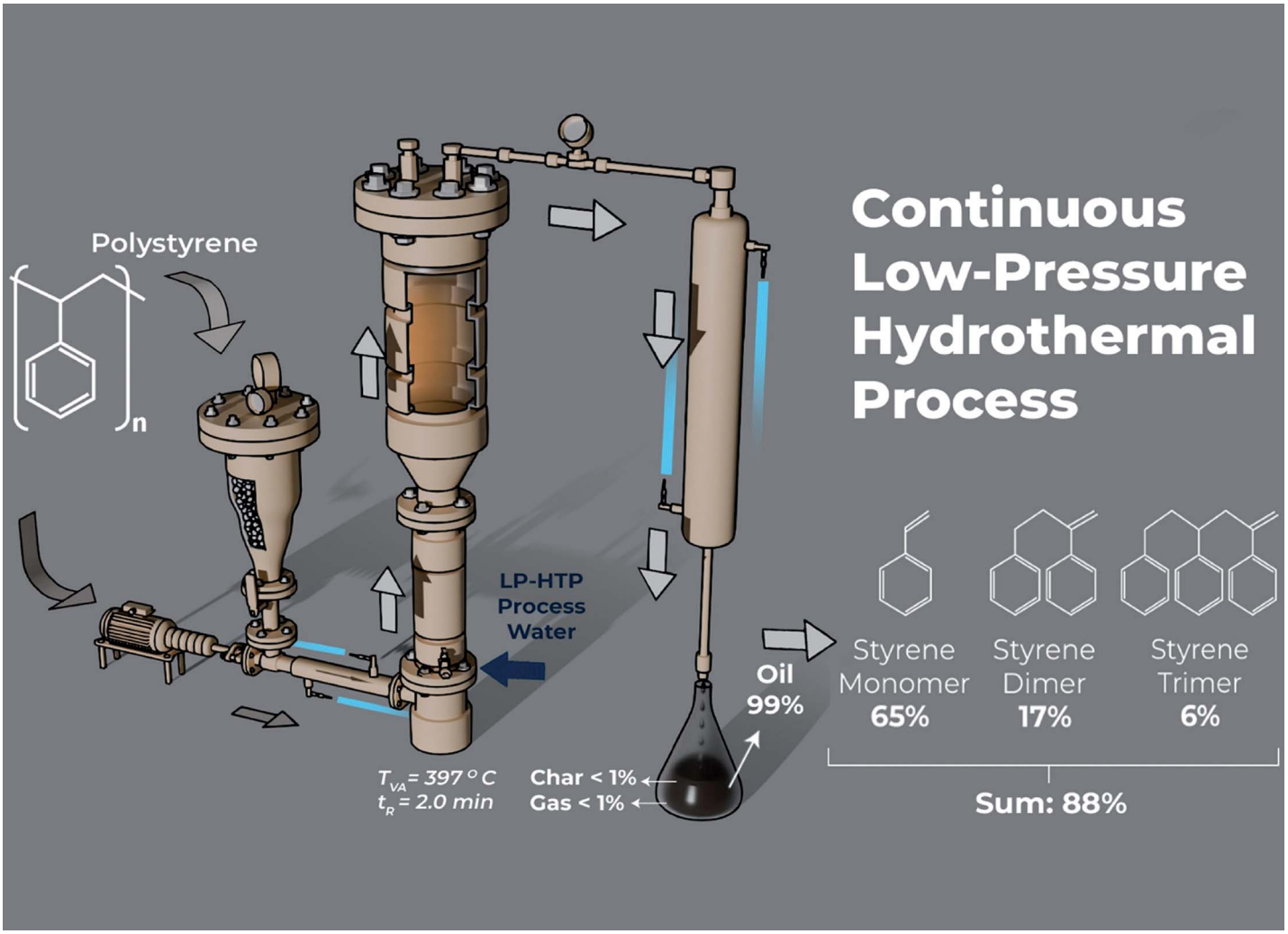

Showcasing research from Professor Wang's laboratory, Davidson School of Chemical Engineering, Purdue University, West Lafayette, Indiana, United States.

Continuous low-pressure hydrothermal processing methods for polystyrene conversion to oils

Exponential growth in the use of plastics since the 1950s has generated over 7 billion tons of waste in the landfills and oceans that degrades slowly, releasing microplastics and thousands of chemicals harmful to life and ecosystems. This study presents a scalable, continuous low-pressure hydrothermal processing (LP-HTP) method to convert one of the plastics, polystyrene, into valuable monomers—requiring no catalysts, producing less char than pyrolysis, operating at 220 times lower pressure than supercritical water liquefaction, and generating 95% lower green-house-gas emissions than incineration. The method has the potential to support a sustainable circular hydrocarbon economy.

Image reproduced by permission of C. Gentilcore, C. Un, P. Vozka, and N.-H. L. Wang from *RSC Sustainability*, 2025, **3**, 3925.

Image illustrated by O. Ozgonul.

As featured in:

See Nien-Hwa Linda Wang *et al.*, *RSC Sustainability*, 2025, **3**, 3925.

ROYAL SOCIETY OF CHEMISTRY

rsc.li/rscsus

Registered charity number: 207890

RSC Sustainability

ROYAL SOCIETY OF CHEMISTRY

PAPER

View Article Online
View Journal | View Issue

Cite this: *RSC Sustainability*, 2025, **3**, 3925

Continuous low-pressure hydrothermal processing methods for polystyrene conversion to oils†

Clayton Gentilcore,[a] Cagri Un,[a] Josue Martinez-Maldonado,[b] Petr Vozka[b] and Nien-Hwa Linda Wang *[a]

Polystyrene (PS) waste is generated at an annual rate of 28 million tons, yet less than 1% is recycled. PS in landfills and ecosystems degrades into microplastics and releases harmful chemicals. This study introduces a continuous low-pressure hydrothermal processing (LP-HTP) method for converting PS into valuable oils without a catalyst. Two continuous reactors were designed, built, and tested at average temperatures from 394 to 538 °C, PS feed rates up to 1.2 kg h^{-1}, and residence times from 0.7 to 3.4 minutes. The process achieved 99 wt% oil yields with minimal gas formation. Water in LP-HTP suppressed char formation to <1 wt%. Lower temperatures and shorter residence times favored styrene production. At 397 °C and 2.0 minutes, the oil contained 65 wt% styrene monomer, and 88 wt% combined styrene monomer, dimer, and trimer. Reaction pathways were proposed based on hydrocarbon species identified *via* GC-MS/FID analyses. A detailed kinetic model was developed using oil composition data from 28 oil samples across three experiments. The model-predicted oil compositions agreed within 6% standard error of the values measured in an independent fourth experiment. The model was used to determine optimal conditions for maximizing styrene product yields. This atmospheric-pressure continuous LP-HTP process is simpler and more cost-effective than batch LP-HTP (2–3 MPa) or supercritical water liquefaction (>22 MPa). It offers a scalable and efficient route to recover valuable monomers from PS waste. It has the potential to reduce PS waste consigned to landfills and mitigate its impact on human health and the environment.

Received 13th December 2024
Accepted 29th June 2025

DOI: 10.1039/d4su00796d

rsc.li/rscsus

Sustainability spotlight

Polystyrene wastes accumulating in landfills and the environment decompose into microplastics and toxic chemicals, resulting in harmful impacts to plants, animals, humans, and entire ecosystems. Conventional plastic waste treatment methods, such as incineration, mechanical recycling, and pyrolysis, have been ineffective in reducing plastic accumulation rates. This study developed continuous low-pressure hydrothermal processing methods for converting polystyrene to valuable oils with minimal char and gas formation. It also features a predictive kinetic model that can be used to increase desired styrene product yields, aiding process optimization and future scale-up. This new technology can help develop a sustainable circular hydrocarbon economy and provide incentives to reduce plastic waste accumulation and associated environmental impacts (UN SDG 12).

1. Introduction

1.1. Background

Global plastic waste generation has increased exponentially since the 1950s, reaching an annual generation rate of 400 million metric tons and an estimated cumulative total of 9 billion metric tons by 2021.[1–3] Only about 10 wt% of this waste has been recycled, and 14 wt% has been incinerated, while the remaining 76 wt% has accumulated in landfills or leaked into the environment.[2,3] Plastics degrade slowly and fragment over decades or centuries into microplastics and nanoplastics, releasing over 16 000 chemicals in the process. Over 4000 of these compounds are known as carcinogens or mutagens, posing serious threats to ecosystems and human health.[2,4,5]

Polystyrene (PS, Type 6) is a common polymer used in packaging, insulation, electronics, and disposable products, and contributes about 7 wt% of global plastic waste each year.[3,6,7] Despite its widespread use, current treatment methods—mechanical recycling, incineration, and pyrolysis—have done little to reduce PS waste accumulation. In 2019, less than 1% of the 28 million metric tons of PS waste generated globally was recycled.[3,8,9] Moreover, PS degradation emits hazardous compounds, such as dioxins, furans, and polycyclic aromatic hydrocarbons (PAHs), which are associated with carcinogenic, mutagenic, and neurotoxic effects.[2,4,5,10,11] These risks underscore the urgent need for more efficient, scalable, and sustainable strategies to manage PS waste and mitigate its environmental and health impacts.

[a]*Davidson School of Chemical Engineering, College of Engineering, Purdue University, West Lafayette, IN 47907, USA. E-mail: wangn@purdue.edu*

[b]*Department of Chemistry and Biochemistry, College of Natural and Social Sciences, California State University, Los Angeles, CA 90032, USA*

† Electronic supplementary information (ESI) available. See DOI: https://doi.org/10.1039/d4su00796d

Table 1 Process conditions and product yields in different methods for polystyrene (PS) treatment or conversion

Method (with best conditions)	Feedstock	Temperature [°C]; residence time [min]	Highest oil [wt%]	Highest total monomer (C_6–C_9) [wt%]	Highest styrene monomer [wt%]	Highest styrene monomer, dimer [wt%]	Highest styrene monomer, dimer, trimer [wt%]	Lowest gas [wt%]	Lowest char [wt%]	Product recovery [wt%]
Landfilling[2–5]	Waste PS	N/A; N/A	N/A; PS waste sent to landfill							0
Mechanical Recycling[3,8,12–14]	Waste PS	170–280; up to 4.0	N/A; PS waste extruded to produce recycled PS product							80–85
Incineration[8,15–17]	Waste PS	650–1650; 0.01–90.0	N/A; PS waste combusted for energy return							35–85
Non-Catalytic Flash Pyrolysis[22]	Commercial PS pellets	450–600; < 0.01	99 (450 °C)	82 (550 °C)	71 (500 °C)	73 (500 °C)	82 (450 °C)	0.4 (450 °C)	None detected (residence time of ∼0.1 s)	95–99
Non-Catalytic Flash Pyrolysis[23]	Virgin PS granules	15–307 in auger, 505–782 in reactor; ≤0.02	99 (15 °C ∼510 °C)	82 (307 °C, ∼629 °C)	74 (15 °C, ∼510 °C)	81 (15 °C, ∼510 °C)	84 (15 °C, ∼510 °C)	1.2 (15 °C, ∼510 °C)	0.1 (residence time of 1 s)	86–99
Non-Catalytic Pyrolysis[24]	Waste PS pellets	450–600; 15.6–47.8	94 (550 °C)	66 (600 °C)	43(600 °C)	44 (600 °C)	45 (600 °C)	0.8 (450 °C)	4.4 (550 °C)	89–94
LP-HTP, experimental (this study)	Commercial PS pellets	T_{VA} = 394–538; t_R = 0.7–3.4	99 (397 °C; 2.0 min)	82 (538 °C; 1.2 min)	65 (397 °C; 2.0 min)	82 (397 °C; 2.0 min)	88 (397 °C; 2.0 min)	0.1 (397 °C; 2.0 min)	0.7 (397 °C; 2.0 min)	95–99
LP-HTP model predictions (6% standard error)	PS	T_{VA} = 300–600; t_R = 0.01–73.7	100	86 (430 °C; 1.7 min)	72 (419 °C; 2.0 min)	79 (411 °C; 1.7 min)	93 (450 °C; 0.2 min)	—		100

1.2. Literature review on methods for polystyrene (PS) treatment

Landfilling polystyrene (PS) waste yields no useful products and poses serious environmental risks, including greenhouse gas emissions and groundwater and soil pollution—factors that can adversely affect wildlife, ecosystems, and the safety of food and water supplies (Table 1).[2–5] Mechanical recycling retains the embodied energy of PS, but polymer degradation limits recyclability to fewer than 10 cycles.[3,8,12–14] Incineration of plastic waste for energy recovery can reclaim up to 85% of the embodied energy of PS (~40 MJ kg^{-1}) in the form of heat and electricity. This recovery, however, is limited to 35% when only electricity is generated.[8,15–17] In addition to its limited efficiency, incineration emits greenhouse gases and toxic compounds that have significant health implications.[8,17–20]

Continuous pyrolysis has emerged as a promising method for converting PS into oils, yet its effectiveness is hindered by char formation (Table S1†).[8,21–24] The accumulation of char leads to catalyst deactivation and equipment fouling, reducing productivity and operational efficiency.[8,25–28] Furthermore, the landfilling or incineration of char releases harmful chemicals to the environment.[18,20,29,30] A comparative summary of operating conditions and product yields for these methods is provided in Table 1. Detailed descriptions of their limitations are included in ESI Text S1.†

Previously, we developed a batch low-pressure hydrothermal processing (LP-HTP) method for converting PS into oils.[30] This approach achieved oil yields as high as 99 wt%, with significantly less char formation compared to pyrolysis. Water played a critical role by acting as a diluent that suppressed polycyclic aromatic hydrocarbon (PAH) reactions responsible for char formation, thereby enhancing oil yields and compositions.[30–32] The function of water in LP-HTP is analogous to that in supercritical water liquefaction (SWL), though batch LP-HTP operates at much lower pressures (2–3 MPa, compared to >22 MPa for SWL), resulting in reduced equipment and operating costs.

Despite these advantages, the batch LP-HTP process was constrained by operation in a pressurized reactor with long heating and cooling cycles, resulting in extended residence times from 19 to 86 minutes.[30] Moreover, monomer (C_6–C_9) yields were limited by reversible reactions with poly-aromatic hydrocarbons (C_{10}–C_{24+}). To describe these interactions, a reversible kinetic model was developed to predict monomer and poly-aromatic yields.[30,33–36] Preliminary assessments suggested that LP-HTP could outperform pyrolysis and incineration in both energy efficiency and environmental impact. However, to date, no study has addressed the development of a continuous LP-HTP process.

1.3. Overall research objective and specific goals

The primary objective of this study is to design and evaluate a continuous LP-HTP system that enhances productivity and efficiency compared to the batch LP-HTP methods, enabling the sustainable conversion of PS waste into high-value oil products. The specific goals of this study are to: (1) Design, construct, and evaluate a mini-pilot-scale continuous low-pressure hydrothermal processing (LP-HTP) system for PS conversion. (2) Investigate the effects of two key operating parameters, temperature and residence time, on oil yields and hydrocarbon compositions. (3) Elucidate reaction pathways by analyzing the detailed hydrocarbon compositions of oils produced under varying operational conditions. (4) Develop a comprehensive kinetic model for PS conversion *via* LP-HTP, incorporating the identified reaction pathways and estimating intrinsic kinetic parameters.

1.4. Research approach and highlights of study

To develop an efficient continuous LP-HTP method, two mini-pilot reactors were designed, constructed, and tested at average temperatures of 394–538 °C, PS feed rates of 0.2–1.2 kg h^{-1}, and residence times from 0.7 to 3.4 minutes. Product samples were collected during steady-state operations lasting 60 to 90 minutes, and the yields of oil, gas, and char were quantified. The hydrocarbon compositions of the resulting oils were characterized through batch distillation and GC-MS/FID analyses. Concentrations of hydrocarbon species were measured in 28 oil samples generated under varying operating conditions across three experiments (Experiments 1–3) to elucidate the kinetic pathways of PS conversion. A plug-flow reactor (PFR) model was developed based on the proposed kinetic pathways and major chemical species present. Intrinsic kinetic parameters were estimated by fitting the model parameters to the experimentally-measured species concentrations from Experiments 1–3. The predictive accuracy of the model was evaluated using four oil samples from an independent experiment (Experiment 4), where the predicted concentrations of the major chemical species agreed with the experimental values within a standard error of 6%. The validated model was then used to identify optimal reaction conditions for maximizing the yields of styrene monomer, total monomers (C_6–C_9), and combined styrene monomer-dimer-trimer. This kinetic model offers a valuable framework for future process optimization and scale-up of continuous LP-HTP systems.

In this study, the first continuous LP-HTP methods were developed for converting PS to high-value oils. The highest oil yield, 99 wt%, was achieved with minimal char and gas formation (<1 wt%) and at a temperature approximately 50 °C lower than that required by non-catalytic pyrolysis (Table 1). The results showed that this oil contained 65 wt% styrene monomer, 17 wt% styrene dimer, and 6 wt% styrene trimer, or a total of 88 wt% styrene monomer, dimer, and trimer. A reactor model based on intrinsic temperature- and equipment-independent kinetic parameters was validated with independent experimental data. Simulations predicted that PS can be converted to various valuable oils, enriched with styrene monomer, dimer, and trimer, for supporting a circular hydrocarbon economy.

2. Experimental materials and methods

2.1. Feedstock used in experiments

Commercial polystyrene (PS) pellets were tested in this study. General-purpose PS pellets (Ultra GPPS 17) with a characteristic diameter of 2–5 mm and reported melt flow rate of 17 grams over 10 minutes were acquired from ResMart (Fort Worth, TX).

A weight-average molecular weight (M_w) of ~156 224 g mol^{-1} (or $C_{12000}H_{12000}$) was estimated (Fig. S1†) from the reported melt flow rate and a literature correlation between PS melt flow rates and molecular weights.[37]

2.2. Equipment design for continuous conversion

Two LP-HTP reactors for continuous conversion of PS were designed, constructed, and tested (Fig. 1). Detailed dimensions of the two reactors are given in the ESI (Fig. S2 and S3†). The reactors were designed for operation at atmospheric pressure (0.1 MPa) to enhance safety and reduce capital and operating costs compared to operating at higher pressures or under vacuum. Both units were designed to operate in a ducted walk-in fume hood for safety (Fig. S2†). Each unit consists of sequential sections for feedstock feeding, feedstock conversion, and product collection. Both units were assembled on an aluminum alloy frame, with identical feeding and collection sections.

The feedstock feeding section of each reactor (Fig. 1, S2 and S3†) was designed to continuously deliver PS pellets to the reactor. Up to 3.9 kg of PS pellets were stored in the 6 L hopper for each experiment. The top of the hopper was sealed with a blind flange prior to operation. The bottom of the hopper was connected to a flanged ball valve to keep the pellets in the hopper prior to feeding. This ball valve opened to the inlet of the auger tube system used to feed PS pellets into the reactor through a flanged pipe connection. The auger blade was like one found in a plastic extrusion setup and was turned within the tube using a 1/8-horsepower gearmotor at rates of up to ~20 RPM during operation to move the PS pellets into the reactor. The packing gland on the auger shaft connecting the blade and the gearmotor prevented leaks from the system. Chilled

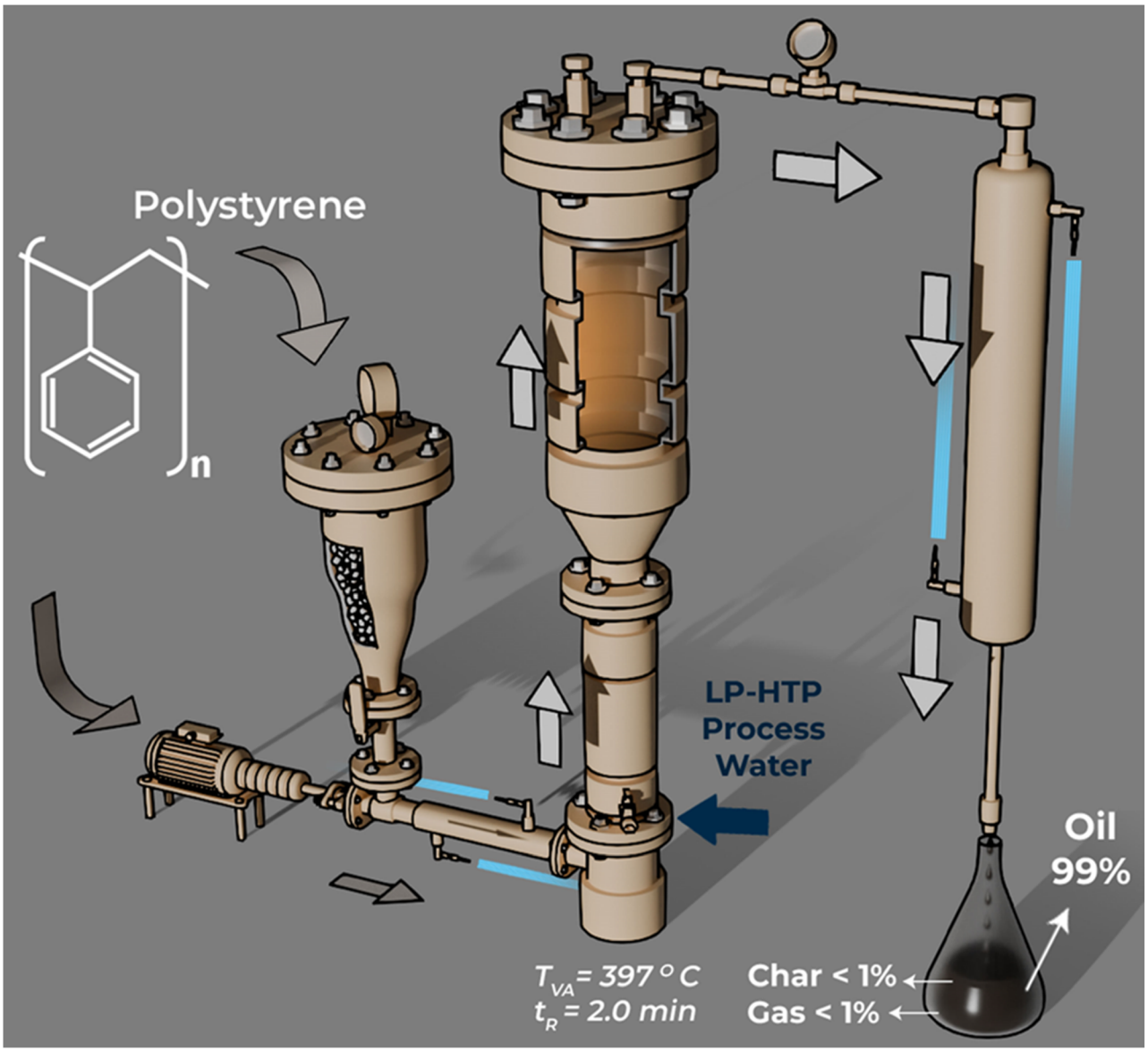

Fig. 1 Schematic diagram of the low-pressure hydrothermal processing Reactor A (~15.1 L) and associated equipment.

water was flowed at ~3 L min^{-1} through the shell pipe surrounding the auger tube using a recirculating chiller (Model #C15-3-2L, Across International, Sparks, NV). The cooling reduces "pellet bridging"—an obstruction of the auger tube inlet caused by polymer melting due to heating from the reactor.[38] As the PS pellets were pushed through the auger tube, the residual heat from the reactor caused the PS entering the reactor to melt.

The conversion section of each mini-pilot reactor (Fig. 1) was designed for continuous conversion of PS to oils. Two reactors with different volumes were designed and constructed to study the impact of varying residence time on oil yields and compositions. In Experiments 1–3, Reactor A (Fig. S3(a)†), with a volume of 15.05 L (rounded up to ~15.1 L), was used; in Experiment 4, Reactor B, with a volume of 4.13 L (rounded up to ~4.2 L), was used (Fig. S3(b)†). Each reactor consisted of a solid collector, a pre-heater, and an upper reactor, with all sections of the reactor well-insulated to minimize heat loss. The solid collector was used for thermal conversion of the PS melt to volatile hydrocarbons (C_1–C_{24+}), and to collect any solids produced during conversion. Water was continuously fed into the reactor through a port near the solid collector to suppress the formation of char during the conversion process. The pre-heater was used to heat the hydrocarbons and process water to the desired temperatures for conversion, and further conversion occurred in the upper reactor. The volatile hydrocarbons produced from PS conversion and the process water used for LP-HTP exited the top of the reactor for product cooling and collection.

The desired operation temperatures in the reactor (Fig. 1) were maintained by using temperature control and monitoring systems. Three thermocouples, $T_{A\text{-}Main}$, $T_{B\text{-}Main}$, and $T_{C\text{-}Main}$, were secured through threaded ports in the reactor wall, to observe the temperatures close to the inner reactor walls for temperature control (Fig. S3(a and b)†). These thermocouples were connected to PID controllers paired with solid state relays that controlled the desired temperatures of different reactor zones by providing power to 208 V heating bands. The bands were grouped together in three zones, with each heating zone paired with a thermocouple (labelled as $T_{A\text{-}Main}$, $T_{B\text{-}Main}$, $T_{C\text{-}Main}$) and connected to the control system (Fig. S3(a and b)†). Additional thermocouples (labelled as $T_{A\text{-}1}$, $T_{A\text{-}2}$, $T_{B\text{-}1}$, $T_{B\text{-}2}$, $T_{B\text{-}3}$) were used to monitor temperatures at additional points inside of each reactor (Fig. S3(a and b)†). Thermocouples were also used to monitor the temperatures of the outer reactor wall where the PS melt entered the solid collector at the auger tip (T_{Tip}) and the chilled water where it exited the auger cooling pipe (T_{Feed}).

The collection section of the mini-pilot unit (Fig. 1, S2 and S3†) allowed produced oils (C_6–C_{24+}) and gases (C_1–C_7) to be cooled to room temperature and then collected continuously. A total condenser was used to cool the produced hydrocarbons and the process water to room temperature. The hydrocarbons and water flowed down through the inner tube as chilled water (5.7 L min^{-1}) flowed countercurrently through the outer shell to cool the products. The products then entered the top of a plugged side-arm flask connected to the condenser. The condensed oil and process water remained in the flask while any produced gas exited through the side-arm, in order to measure the gas flow rate by using a gas flow meter.

2.3. Experimental procedures

The start-up, operation, and shut-down methods for continuous LP-HTP operation were designed and tested in four experiments. Detailed experimental procedures are described in ESI Text S2.† After assembling and insulating the reactor (Fig. 1, S2 and S3†), the unit was contained within the walk-in fume hood. The hopper was filled with pre-weighed PS pellets, and the unit was purged with nitrogen gas to prevent combustion. As in the previous batch LP-HTP study, process water was purified using a Milli-Q water purification system.[30] The process water was delivered to the reactor using a calibrated peristaltic pump. A recirculating chiller was used to deliver chilled water to the auger tube system and the total condenser during the entire experiment.

When increasing the inner reactor temperatures and reaching steady-state temperatures for PS conversion during start-up, the solid collector on the bottom of the reactor was heated to ~375 °C while the higher reactor sections were heated to the desired set temperature for each experiment. The minimum temperature for PS thermal decomposition was reported previously to be 300 °C.[23,30] Operation at ~375 °C allowed for fast thermal decomposition of PS in the solid collector while minimizing "pellet bridging" in the auger tube.[38]

Once the desired temperatures were reached and remained steady, a pre-weighed side-arm flask for product collection was connected to the condenser outlet and the gas flow meter. Then, the PS pellets were fed into the reactor by using the motorized auger. When hydrocarbon gases and oil were initially observed entering the side-arm flask during this initial PS feeding (Fig. S4–S7†), the peristaltic pump for delivering process water was turned on and the associated reactor port was opened, allowing for LP-HTP conversion to begin. After 30 minutes of PS feeding, the side-arm flask connected to the unit was swapped out with an additional pre-weighed side-arm flask, starting the "Sample 1" collection period for each experiment.

During operation, sample collection periods lasting 30 minutes were used for collecting oils and used process water from the continuous LP-HTP unit and measuring produced gas flow rates. The temperatures, auger rotation rate, mass of process water fed into the reactor, and flow rate of produced gas were recorded every five minutes. Furthermore, gas collection bags were used to collect produced gases during designated collection periods. At the end of each sample collection period of 30 minutes, a new collection flask was attached to the reactor. Each flask containing oil and process water was weighed, and the liquid contents were transferred to a glass bottle. Product collection would continue until either pellet bridging occurred in the auger tube to prevent feeding or the PS pellets were completely consumed. Upon completion of product collection and process shut-down procedures, the mini-pilot unit was disassembled and cleaned after each experiment.

Table 2 Volume-average temperatures (T_{VA}), residence times (t_R), PS and process water feed rates, oil production rates, total operation time, steady-state duration, and steady-state oil production rate for Experiments 1–4

Purpose for kinetic model	Exp.#	T_{VA} [°C]	t_R [min]	PS feed rates [kg h^{-1}]	Water feed rate [kg h^{-1}]	Oil production rates [kg h^{-1}]	Total operation time [min] (# of samples)	Steady-state duration [min] (sample identities)	Steady-state oil production rate [kg h^{-1}]
Reaction pathway and model development Model validation	1	394–397	2.0	1.02–1.03	0.05	1.01–1.02	60 (2 samples)	60 (1–1 to 1–2)	1.01 ± 0.01
	2	479–483	1.4–3.4	0.21–1.18	0.05	0.20–1.15	360 (12 samples)	60 (2–4 to 2–5)	0.59 ± 0.02
	3	536–538	1.2–1.9	0.21–0.77	0.10	0.20–0.74	420 (14 samples)	90 (3–3 to 3–5)	0.65 ± 0.03
	4	479–483	0.7–0.8	0.35–0.49	0.05	0.33–0.47	120 (4 samples)	90 (4–2 to 4–4)	0.34 ± 0.01

2.4. Experimental design

Four continuous LP-HTP experiments were designed and conducted at various reaction temperatures, residence times, PS feed rates, and process water feed rates to examine the impacts of different reaction conditions on oil yields and compositions (Table 2). Experiments 1–3 were conducted to understand the kinetic pathways and develop a kinetic model for continuous PS conversion. The compositions of the oil samples from the experiments were used to develop PS conversion pathways in Section 3. The results were also used for estimating the best-fitting intrinsic parameters for the kinetic model (Section 4.1 and 4.2). The oil compositions of Experiment 4 were used to validate the kinetic model and intrinsic parameters (Section 4.3).

The operating conditions for the four experiments are shown in Table 2. The experiments were conducted at atmospheric pressure (0.1 MPa) to ensure process safety and scalability. A total of 32 oil samples were collected during operation across thirty-two collection periods, each lasting 30 minutes. Steady-state operation was defined as when the variation of PS feed rate was within ±10% between the sampling periods. The first three experiments, Experiments 1–3, were conducted using the 15.1 L Reactor A. Experiment 4 was conducted using the 4.2 L Reactor B.

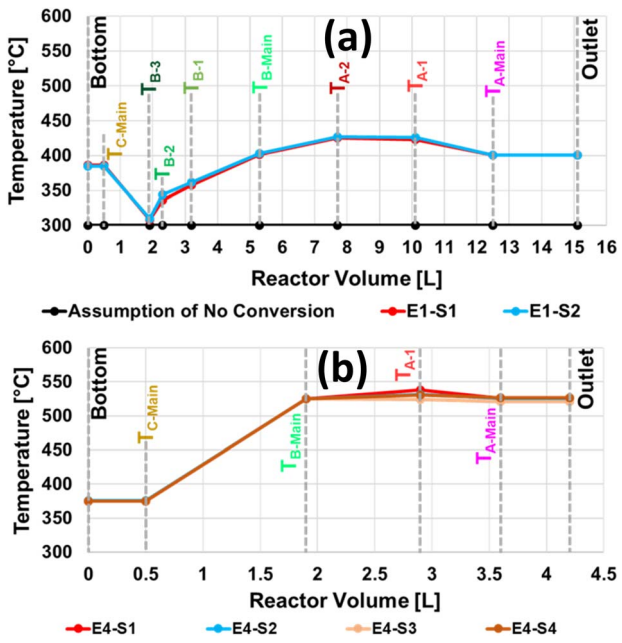

Fig. 2 Volumetric temperature profiles for (a) the 2 sample collection periods of Experiment 1 (E1-S1 to E1-S2) and (b) the 4 sample periods of Experiment 4 (E4-S1 to E4-S4).

A volume-average temperature (T_{VA}) for each sample period was estimated based on the temperatures measured using the thermocouples located in each reactor (Fig. S4–S7†). Temperatures within the reactor volume between each thermocouple were assumed to vary linearly between the measured temperatures (Fig. 2(a and b) and S8(a and b)†). For Reactors A and B, with respective volumes of 15.1 L and 4.2 L (Fig. 1, S2 and S3†), temperatures were approximated for every 0.1 L, respectively resulting in 151 and 42 temperature data points. From these temperature profiles, the volume-average temperatures (T_{VA}) were estimated (Table 2). Residence times (t_R) for each sample were estimated based on the times required for the hydrocarbons and process water to pass through all 0.1 L volumetric slices of the reactor used. The respective vapor phase density data sets for toluene and water were used to estimate the volumetric flow rates for hydrocarbons with various molecular weights and process water in each volumetric slice.[39] The estimated values of T_{VA} and t_R are summarized in Table 2 and shown for each sample in Sections 3 and 4.

Experiment 1 was conducted at temperatures like those of the previous batch LP-HTP study to study the impact of low residence times on styrene monomer (C_8H_8) and total monomer (C_6–C_9) yields from PS conversion.[30] Experiments 2 and 3 were conducted to study the impact of higher operation temperatures on styrene monomer (C_8H_8) and total monomer (C_6–C_9) yields. Experiments 2 and 3 were used to also study the impact of varying residence times on oil yields and compositions. In Experiment 3, a higher process water feeding rate of 0.10 kg h^{-1} was used to study the impacts of shorter residence time on PS conversion (Table 2).

The results of Experiments 1–3 were used for developing a kinetic model for predicting product yields as a function of temperature and residence time (Table 2). In Experiment 4, the smaller 4.2 L Reactor B was used to study the impacts of shorter residence time on oil yields and oil compositions. The results were also compared with model predictions for testing and verifying the proposed pathways and the kinetic model parameters estimated using Experiments 1–3.

2.5. Product collection and yield estimation procedures

Following process shut-down, any unconverted PS present in the hopper and the auger tube were collected and weighed. The

mass of PS converted during each experiment was estimated based on the difference between the mass of PS pellets fed into the hopper before the experiment and the mass of the remaining PS collected after the experiment. The converted PS was estimated to be equivalent to the sum of the total mass of gas, char, and oil produced in each experiment (eqn (1a)). The mass of PS converted during each sample period was estimated to be based on the sum of the gas, char, and oil produced for each sample (eqn (1b)). Furthermore, the sum of specific product masses from the samples was assumed to be equal to the total mass of each product from the experiment (eqn (1c)–(1f)).

$$m_{\mathrm{PS_{Converted_{Total}}}} = m_{\mathrm{Gas_{Total}}} + m_{\mathrm{Char_{Total}}} + m_{\mathrm{Oil_{Total}}} \quad (1a)$$

$$m_{\mathrm{PS_{Converted_y}}} = m_{\mathrm{Gas_y}} + m_{\mathrm{Char_y}} + m_{\mathrm{Oil_y}} \quad (1b)$$

$$m_{\mathrm{PS_{Converted_{Total}}}} = \sum m_{\mathrm{PS_{Converted_y}}} \quad (1c)$$

$$m_{\mathrm{Gas_{Total}}} = \sum m_{\mathrm{Gas_y}} \quad (1d)$$

$$m_{\mathrm{CharTotal}} = \sum m_{\mathrm{Chary}} \quad (1e)$$

$$m_{\mathrm{OilTotal}} = \sum m_{\mathrm{Oily}} \quad (1f)$$

Total = total in experiment, y = specific sample in experiment.

To confirm the mass balance for each experiment, the weights for the produced gas were estimated. The yield of the gas produced in each sample was estimated based on data recorded from the gas flow meter. For each sample period of 30 minutes, the gas flow meter readings were recorded every 5 minutes to obtain an average estimated gas flow rate per sample. As mentioned in Section 2.3, gas collection bags were used to collect gas samples during PS conversion for analysis. Following GC-FID analysis of the gas samples (Tables S2, S3, and Fig. S9†) collected during Samples E2-S5, E3-S2, E3-S6, and E3-S11, the average molecular weights of the different gas samples were estimated to be like that of ethane (C_2H_6). Then, the ethane density at 25 °C and the average gas flow rate during each sample collection period were used to calculate the mass of gas produced during each sample period (eqn (2a)).[39]

The char yield from each experiment was estimated by directly weighing the char remaining in the reactor after conversion. By opening the top of the reactor after cooling it to room temperature and cleaning the inside of the reactor with a brush, any char produced was collected in the attached solid collector section (Fig. 1). The char was removed from the solid collector and weighed to estimate its total yield for the experiment. The percentage yield of char for each sample of the experiment was assumed to be equal to this total percentage yield of char measured (eqn (2b)).

The oil yield from each sample was estimated from the difference between the mass of the converted PS and the masses of the produced gas and char (eqn (2c)).[30–32] As described in Section 2.3, each sample containing produced oil and used process water was collected from the mini-pilot unit in a pre-weighed side-arm flask. After removal from the unit, the side-arm flask was weighed to determine the mass of oil and water collected. The recorded mass of process water fed into the reactor during the specific sample period was subtracted from this mass to estimate the amount of oil collected. The total mass of oil collected during each experiment was about the same, within 1%, as the total oil mass estimated by the difference between the masses of converted PS and produced gas and char (eqn (2c)). This agreement indicates the accuracy of the mass balance and the oil yield estimation for each experiment.

$$\text{Gas yield\% of sample y} = \left[\frac{m_{\mathrm{Gas_y}}}{m_{\mathrm{PS_{Converted_y}}}}\right] \times 100\% = \left[\frac{\dot{V}_{\text{Avg Gas Flow}_y} \times t_y \times \rho_{C_2H_6,\ 25\ ^\circ C}}{m_{\mathrm{PS_{Converted_y}}}}\right] \times 100\% \quad (2a)$$

$$\text{Char yield\% of sample y} = \left[\frac{m_{\mathrm{Char_{Total}}}}{m_{\mathrm{PS_{Converted_{Total}}}}}\right] \times 100\% = \left[\frac{m_{\mathrm{Char_y}}}{m_{\mathrm{PS_{Converted_y}}}}\right] \times 100\% \quad (2b)$$

$$\text{Oil yield\% of sample y} = \left[\frac{m_{\mathrm{Oil_y}}}{m_{\mathrm{PS_{Converted_y}}}}\right] \times 100\% = \left[\frac{m_{\mathrm{PS_{Converted_y}}} - m_{\mathrm{Gas_y}} - m_{\mathrm{Char_y}}}{m_{\mathrm{PS_{Converted_y}}}}\right] \times 100\% \quad (2c)$$

Total = total in experiment, y = specific sample in experiment.

2.6. Oil analysis by distillation and GC-MS/FID methods

The oil compositions were determined using similar methods used in the previous batch LP-HTP study on PS conversion.[30] Batch distillation and subsequent GC-MS/FID analyses were used to study the composition of the produced oils. Before distillation, the oils were separated from water by gravity separation and treated with $MgSO_4$ to remove any trace water, and 2 grams of each oil sample were used for GC-MS/FID analysis. Based on the ASTM D86 distillation method,[40] up to 100 grams of oil were separated into three fractions. The first recovered oil fraction ($T_{\mathrm{Distillation}} \leq 170$ °C) mostly contained one-ring aromatic hydrocarbons, or "monomers" (C_6–C_9). The second fraction (170 °C < $T_{\mathrm{Distillation}} \leq 300$ °C) mostly contained two-ring aromatic hydrocarbons, or "dimers" (C_{10}–C_{16}). The third fraction, remaining in the 250 mL round bottom flask after distillation (300 °C < $T_{\mathrm{Distillation}}$), contained mostly three-ring aromatic hydrocarbons, or trimers (C_{14}–C_{24+}), and heavier poly-aromatic hydrocarbons. The third fraction was labelled as "heavy aromatics" in the experimental results. The oil fraction yields reported in this study were based on the weights of these oil fractions recovered from distillation.

Specific oil samples in each experiment were distilled to allow the hydrocarbon distribution of other samples to be estimated. Samples E1-S1 and E1-S2 (or 1-1 and 1-2) were distilled for Experiment 1. Samples 2-1, 2-2, 2-5, 2-8, and 2-11 were distilled for Experiment 2. Samples 3-2, 3-6, 3-10, and 3-14

were distilled for Experiment 3, and Samples 4-1 and 4-4 were distilled for Experiment 4. For all other samples from each experiment, the weight percentages of the lighter oil (sum of Fraction 1 and Fraction 2) were estimated from linear correlations with oil collection rates as explained in the ESI (Fig. S10, and Table S4†).

As in the previous batch LP-HTP study,[30] the composition of each oil sample produced from PS conversion was determined using GC-MS/FID methods (Table S5†).[41,42] The analysis identified chemical species in the C_6–C_{24} range in each oil sample. Some heavier poly-aromatic hydrocarbons, however, were too heavy to be detected with GC-MS/FID. Therefore, any heavier poly-aromatic hydrocarbons present in the "heavy aromatic" fraction by weight were assumed to be C_{24+}.

3. Results of continuous PS conversion

3.1. Development of reaction pathways from results of Experiment 1

In our previous batch LP-HTP study, complete PS conversion to oils at an average reaction temperature of 341 °C was observed after 19 minutes. Yields of styrene were quite sensitive to the temperature and the reaction time. At an average temperature range between 376 and 428 °C, the yields of the monomers (C_6–C_9) and the poly-aromatics (C_{10}–C_{24+}) reached constant values, indicating reversible reactions between the two species. In the previous study, only composition data for long residence times of 19–86 min could be obtained.[30] Therefore, to investigate the early stage of the reaction pathways, Experiment 1 was conducted at low average temperatures of 394–397 °C and a short residence time of 2.0 min. The temperature profiles of Experiment 1 are shown in Fig. 2(a).

In Experiment 1, two oil samples were produced. PS was fed at a steady-state rate of ~1 kg h^{-1}, and water was fed at 0.05 kg h^{-1} to achieve a 5 wt% water loading (Table 2). After collecting two samples, Sample 1-1 and Sample 1-2, pellet bridging in the auger caused PS feeding to stop, ending the experiment (Fig. S4†).

The results in Fig. 3 show high oil yields of 99 wt% and minimal gas and char yields (<1 wt%). The yields of oil, gas, and char of the two samples agree within 1%. Individual yields of monomers, 67–69 wt%, dimers, 21–22 wt%, and heavy aromatics, 9–10 wt%, in the two samples agreed within 2%. The individual yields of styrene monomer, dimer, and trimer agreed to within 4 wt%. These reproducible results in all yield categories indicate steady-state operation for 60 minutes.

The oil compositions for the two samples from Experiment 1 are shown in Fig. 4(a). Sample 1-1 had a high combined yield of 88 wt% of the three styrene compounds, including 65 wt% styrene monomer, 17 wt% styrene dimer, and 6 wt% styrene trimer (Table S6†). The results suggest that the PS conversion in this process begins with fast thermal decomposition of PS to form trimers at short residence times.

Plausible reaction pathways were proposed in Fig. 4(b), based on these observations and literature data.[23,24,30,43–47] The PS polymer would initially decompose into styrene trimers by random chain scission and hydrogen transfer. The styrene trimer would then decompose into a styrene dimer and a styrene monomer. The styrene dimer would further convert into two styrene monomers.

It was proposed that a styrene dimer could also decompose into non-styrene monomers (C_6–C_9, Fig. 4(a and b)).[23,24,30,46–48] The non-styrene monomers included BTEX chemicals such as benzene (light green, C_6), toluene (green, C_7), and ethylbenzene (dark green, C_8), and other monomers such as α-methylstyrene (yellow, C_9), as shown in Fig. 4(a). Some styrene monomers could decompose into non-styrene monomers and potentially form light hydrocarbon gases (C_1–C_7).[30] The non-styrene monomers could then combine to form non-styrene poly-

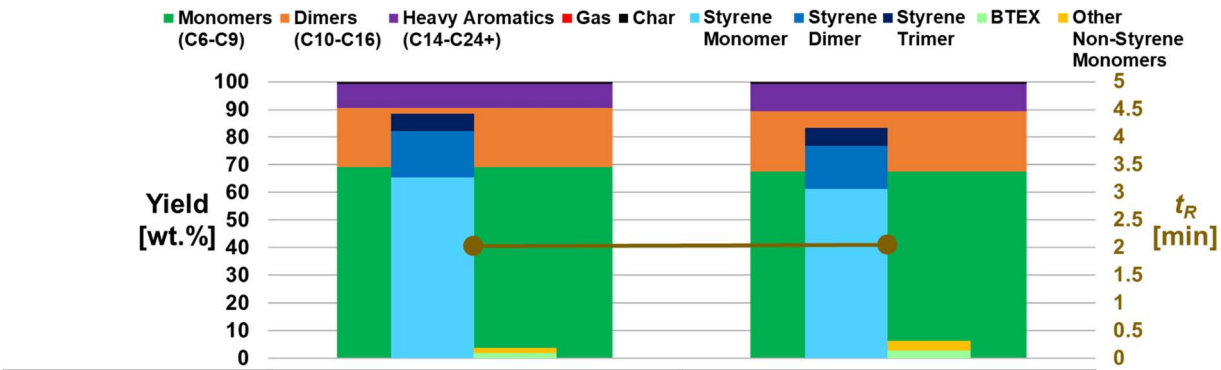

Sample #	1-1	1-2
T_{VA} [°C]	397	394
T_{Range} [°C]	307 to 432	308 to 427
PS Feed Rate [kg/hr]	1.03	1.02
Water Feed Rate [kg/hr]	0.05	

Fig. 3 Yields of oil, gas, and char in sample collection periods of Experiment 1, with temperatures, residence times, feed rates, and oil compositions shown.

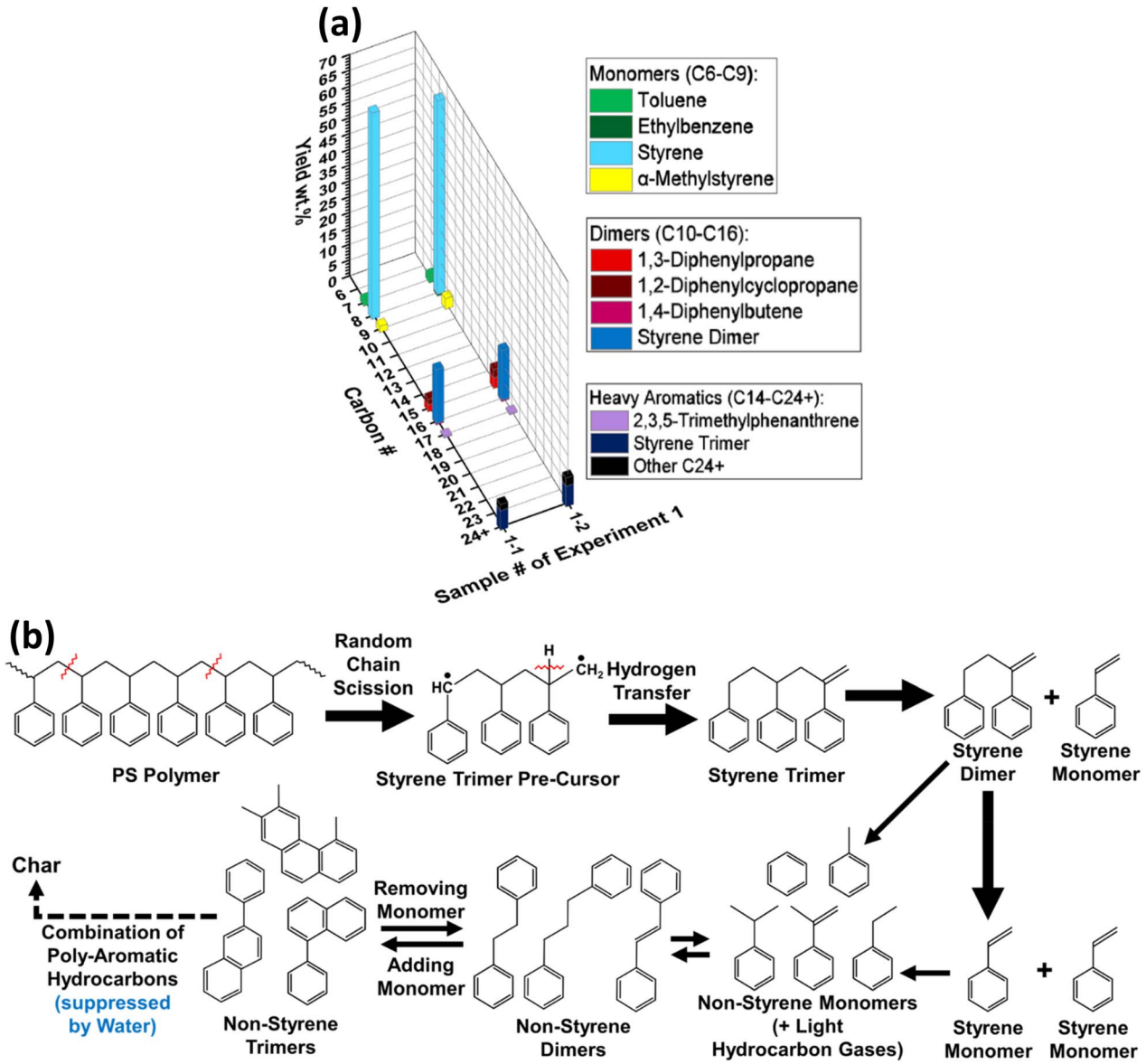

Fig. 4 (a) Detailed compositions of oils from Experiment 1. (b) Reaction pathways proposed for PS conversion in this study.

aromatics (C_{10}–C_{24+}) that can decompose into non-styrene monomers in a reverse reaction.[30] The poly-aromatics in Experiment 1 included dimers (reds and pinks, C_{15}–C_{16}), trimers (purple, C_{17}), and heavier non-styrene poly-aromatic hydrocarbons (black, C_{24+}). These reaction pathways, supported by the data in Fig. 4(a), were used in the development of the kinetic model proposed in Section 4.

3.2. Effects of temperature and residence time on results of Experiments 2 and 3

Two additional experiments were conducted to study the effects of temperature and residence time on the oil yields and the oil compositions in continuous PS conversion. In Experiments 2 and 3, the oil production rate decreased gradually during the respective production periods of 6 hours and 7 hours due to decreasing PS feeding rates (Fig. S5 and S6†).

Experiment 2 was conducted at higher T_{VA} of 479–483 °C and a wider t_R range of 1.4–3.4 min than Experiment 1 (Table 2), with 12 samples collected and analyzed. The high temperature in Experiment 2 resulted in high oil yields, 96–98 wt%, with minimal yields of gas (1–2 wt%) and char (1 wt%) (Fig. 5(a)). The total monomer (C_6–C_9) yields, 75–77 wt%, were higher than in Experiment 1. Styrene monomer yields, however, were lower, 47–59 wt%, and decreased with increasing residence time. Only trace amounts of styrene dimer were detected in Samples 2-1 to 2-3, which had shorter residence times, 1.4–2.0 min, than the remaining samples. No styrene trimer was observed in Experiment 2.

The trends of higher yields of total monomers and lower yields of styrene compounds in the oils from Experiment 2 (Fig. 5(b) and Table S7†) support the proposed kinetic pathways (Fig. 4(b)). At higher T_{VA} of 479–483 °C than in Experiment 1, the styrene dimers and trimers were more readily converted to monomers, and styrene monomers were more readily converted

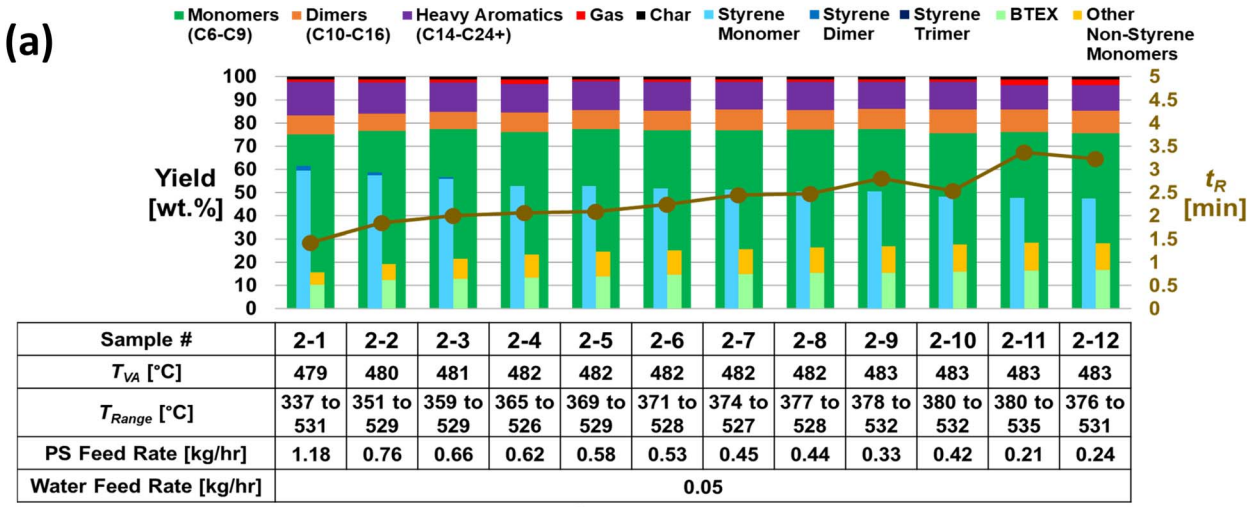

Sample #	2-1	2-2	2-3	2-4	2-5	2-6	2-7	2-8	2-9	2-10	2-11	2-12
T_{VA} [°C]	479	480	481	482	482	482	482	482	483	483	483	483
T_{Range} [°C]	337 to 531	351 to 529	359 to 529	365 to 526	369 to 529	371 to 528	374 to 527	377 to 528	378 to 532	380 to 532	380 to 535	376 to 531
PS Feed Rate [kg/hr]	1.18	0.76	0.66	0.62	0.58	0.53	0.45	0.44	0.33	0.42	0.21	0.24
Water Feed Rate [kg/hr]	0.05											

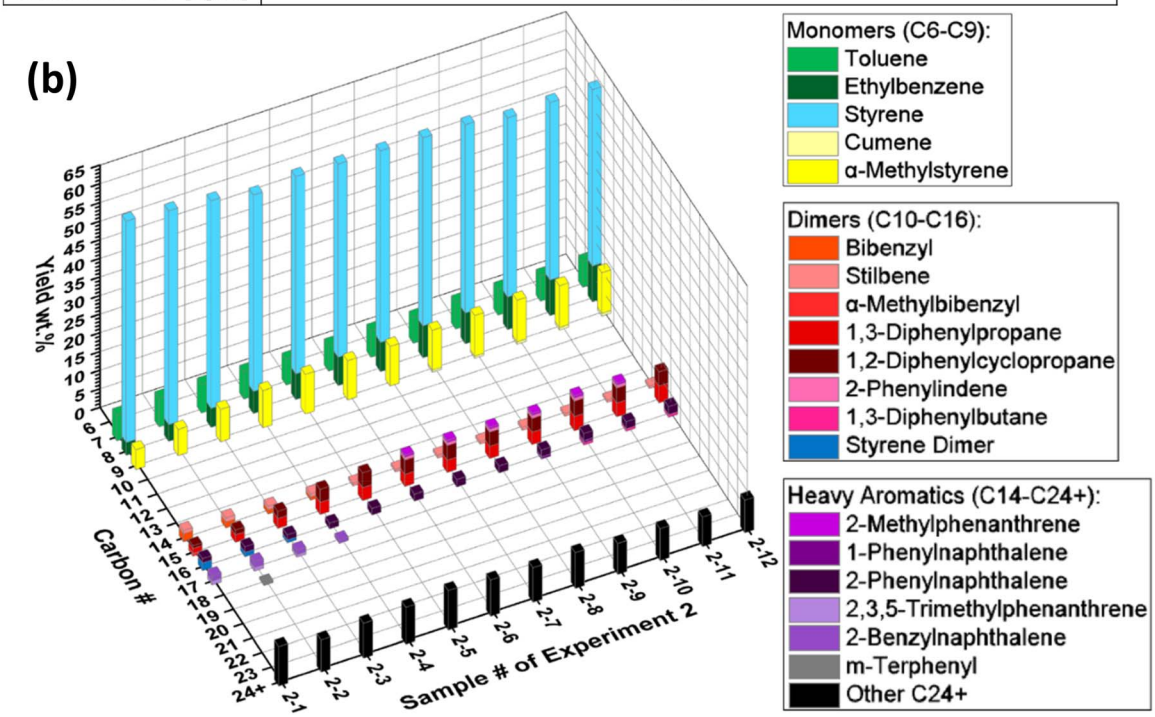

Fig. 5 (a) Yields of oil, gas, and char in sample collection periods of Experiment 2, with temperatures, residence times, feed rates, and oil compositions shown. (b) Detailed compositions of oils from Experiment 2.

to non-styrene compounds. Furthermore, the comparison of oil compositions of samples from Experiment 2 indicates that a longer residence time allowed more styrene compounds to convert to non-styrene compounds. Longer t_R also allowed reactions between non-styrene monomers and non-styrene poly-aromatics to form new compounds, such as cumene (light yellow, C_9), 2-phenylindene (light pink, C_{15}), 1,3-diphenylbutane (pink, C_{16}), 2-methylphenanthrene (light purple, C_{15}), and 1-phenylnaphthalene (purple, C_{16}). Compared to Experiment 1, however, yields of heavier non-styrene poly-aromatics (black, C_{24+}) increased from 2–3 wt% to 8–11 wt%. These results suggest that lower operation temperatures and residence times can help increase the total yields of styrene monomers, dimers, and trimers, and reduce the production of heavier poly-aromatics, the precursors of char.

The trends of high oil yields and varying oil compositions with increasing T_{VA} and t_R were also observed in Experiment 3, conducted at the highest T_{VA} in this study of 536–538 °C for t_R of 1.2–1.9 min (Table 2). In this experiment, 14 oil samples were collected, with high oil yields of 95–97 wt%, and yields of 1–2 wt% gas and 2 wt% char (Fig. 6(a)). The char formation was kept low at this high temperature due to the diluent effect of water. The highest T_{VA} of Experiment 3 resulted in the highest observed total monomer yield of 82 wt%. However, the styrene monomer yield decreased from 57 wt% to 34 wt% from Sample 3-1 to 3-14, as styrene monomers were converted to non-styrene monomers with the increasing residence time.

The effects of higher T_{VA} and increasing t_R on the oil compositions of Samples 3-1 to 3-14 are shown in Fig. 6(b). As in Experiment 2, styrene monomer yields decreased with

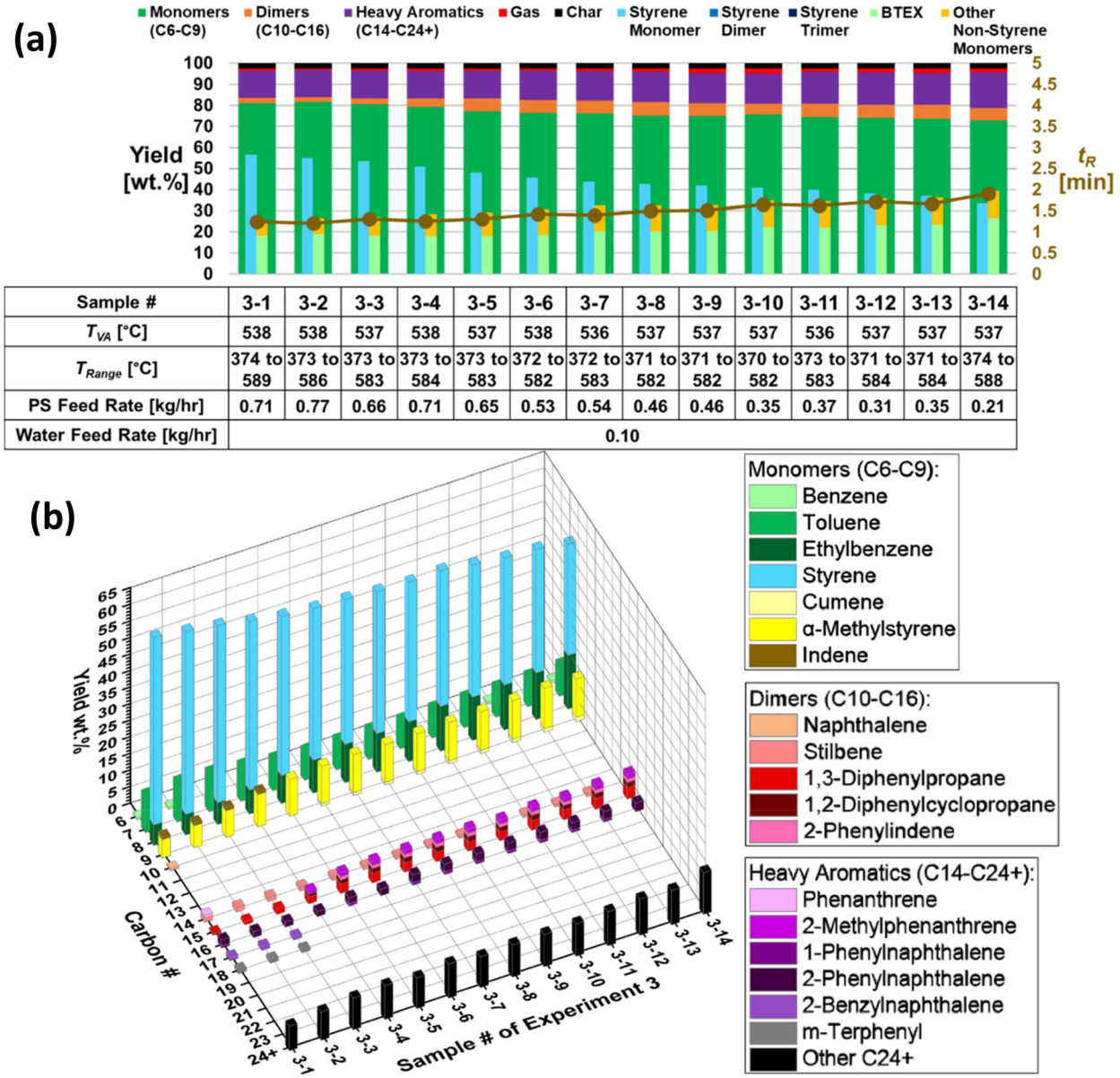

Sample #	3-1	3-2	3-3	3-4	3-5	3-6	3-7	3-8	3-9	3-10	3-11	3-12	3-13	3-14
T_{VA} [°C]	538	538	537	538	537	538	536	537	537	537	536	537	537	537
T_{Range} [°C]	374 to 589	373 to 586	373 to 583	373 to 584	373 to 583	372 to 582	372 to 583	371 to 582	371 to 582	370 to 582	373 to 583	371 to 584	371 to 584	374 to 588
PS Feed Rate [kg/hr]	0.71	0.77	0.66	0.71	0.65	0.53	0.54	0.46	0.46	0.35	0.37	0.31	0.35	0.21
Water Feed Rate [kg/hr]	0.10													

Fig. 6 (a) Yields of oil, gas, and char in sample collection periods of Experiment 3, with temperatures, residence times, feed rates, and oil compositions shown. (b) Detailed compositions of oils from Experiment 3.

increasing t_R in Experiment 3, because of the conversion into non-styrene monomers. The increased production of non-styrene monomers led to increased yields of non-styrene poly-aromatics, increasing from 16 wt% to 24 wt% from Sample 3-1 to 3-14 (Table S8†). Moreover, since Experiment 3 was done at higher average temperatures than those of Experiment 2 (Table 2), higher yields of heavier poly-aromatics (black, C_{24+}), 7–13 wt%, were observed. These results further suggest that lower temperatures and residence times are needed to minimize the production of heavier poly-aromatics.

Overall, the results of Experiments 1–3 and the proposed reaction pathways indicate that with increasing T_{VA} and t_R, more styrene dimers and styrene monomers convert into non-styrene monomers, and more non-styrene poly-aromatics form. Therefore, to increase the yields of desired styrene compounds and to reduce the complexity of oils produced, the LP-HTP conversion of PS should be conducted at lower T_{VA} and t_R. The proposed pathways of Fig. 4(b) were the basis for the kinetic model developed in Section 4.

4. Kinetic model development and estimation of intrinsic kinetic parameters

The purpose of developing a kinetic model for continuous LP-HTP was to aid process optimization and future scale-up efforts. In our previous batch LP-HTP study, a kinetic model

was developed based on the data obtained for long reaction times of 19–86 min. Although the temperature histories were considered in developing the kinetic model, no samples could be obtained at short reaction times needed to identify the species produced in the early stages of PS conversion.[30] The continuous LP-HTP equipment in this study enabled obtaining samples from runs with shorter residence times (0.7–3.4 min). Thus, the previous kinetic model from the batch study was expanded to include the early-stage reactions (Fig. 4(b)). The oil compositions from Experiments 1–3 were used for estimating the intrinsic parameters of the kinetic model.

For simplicity, in the new kinetic model, the hydrocarbon species observed in Experiments 1–3 (Fig. 4–6) were combined to five major chemical species (Section 4.1). The best-fitting kinetic parameters were estimated based on the temperatures, residence times, and yields of the chemical species obtained from the 28 samples of Experiments 1–3 (Section 4.2). The predictions of the kinetic model were tested and validated with data from an independent experiment, Experiment 4 (Section 4.3). The kinetic model, with the validated parameters, was used to generate yield predictions as a function of temperature and residence time in Section 5.

4.1. Equations of kinetic model for continuous PS conversion

The proposed kinetic pathways for PS conversion (Fig. 4(b)) were used as the basis for the new kinetic model (Fig. 7). The hydrocarbon species obtained from the GC-MS/FID analyses were classified into five major chemical species, styrene trimer ($C_{24}H_{24}$), styrene dimer ($C_{16}H_{16}$), styrene monomer (C_8H_8), lumped non-styrene monomers (C_6–C_9), and lumped non-styrene poly-aromatics (C_{10}–C_{24}). The lumped poly-aromatics consisted of non-styrene dimers (C_{10}–C_{16}) and heavy aromatics (C_{14}–C_{24+}). The molecular weights of the two lumped species in the model were based on average values, with the molecular weight of C_8H_8 assigned to non-styrene monomers and that of $C_{16}H_{16}$ assigned to non-styrene poly-aromatics.

As in our previous batch LP-HTP study,[30] the new kinetic model was assumed to consist of first-order reactions for decomposition and second-order reactions for chemical combination (Fig. 7). Since the PS polymer fed into the reactor decomposed quickly, the starting compound of the kinetic model was assumed to be styrene trimer (eqn (3)). The trimer would decompose into a styrene dimer and a styrene monomer (k_T). This conversion was followed by the parallel reactions of a styrene dimer converting to two styrene monomers (k_{D1}) or two non-styrene monomers (k_{D2}). The resulting styrene monomers would then convert into non-styrene monomers (k_M). As observed in the previous batch LP-HTP study, the yields of the monomers and the poly-aromatics plateaued because of reversible reactions between non-styrene monomers and non-styrene poly-aromatics. Therefore, the kinetic model also included reversible reactions for the second-order combination of two non-styrene monomers into one non-styrene poly-aromatic (k_{PA}) and first-order decomposition of one non-styrene poly-aromatic into two non-styrene monomers (k_{PB}). Gas or char formation was neglected in this model since minimal yields (≤2 wt% gas, ≤2 wt% char) were observed in Experiments 1–3.

$$F_{\mathrm{PS_{Convertedy}}} = \frac{12\,000}{24}F_{\mathrm{StyTri_i}} = \frac{12\,000}{24}F_{\mathrm{StyTri_f}} + \frac{12\,000}{16}F_{\mathrm{StyDi_f}} + \frac{12\,000}{8}F_{\mathrm{StyM_f}} + \frac{12\,000}{8}F_{\mathrm{NonSM_f}} + \frac{12\,000}{16}F_{\mathrm{Poly_f}} \quad (3)$$

The molar flow rates and the concentrations of the five species and process water were used with the kinetic constants in the model (Fig. 7). The model consisted of a molar flow balance equation (eqn (4)) and rate law equations with kinetic constants, which were assumed to follow the Arrhenius

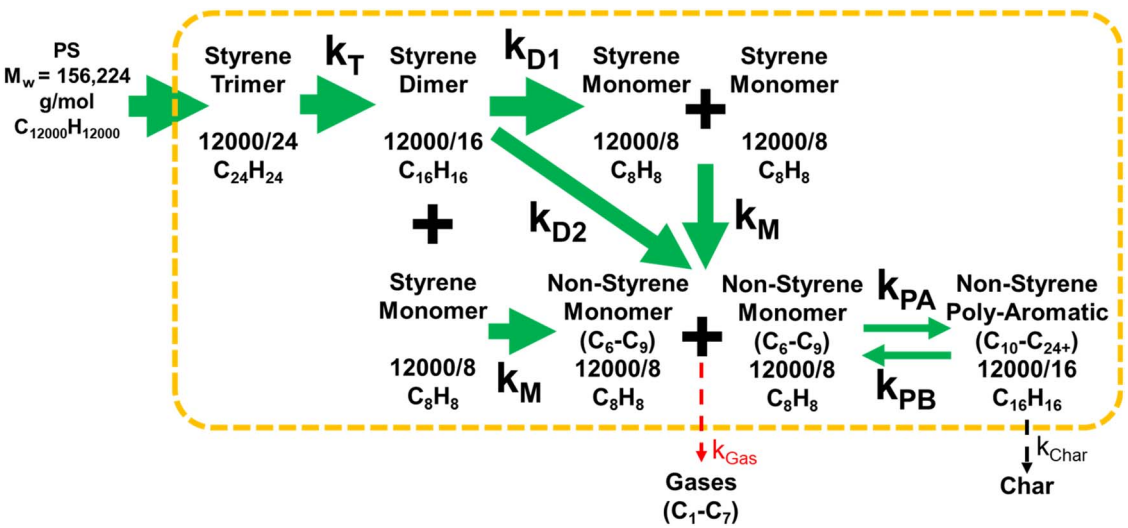

Fig. 7 Proposed kinetic model to describe PS conversion in continuous LP-HTP.

equation (eqn (5)). The rate law equations were derived based on gas-phase plug-flow reactor (PFR) behavior with no pressure drop. The conversion process was modelled to occur across a series of 0.1 L volumetric sections representing the total volume of the reactor used, such as 151 volumetric slices of 0.1 L for the 15.1 L Reactor A. The total concentration of hydrocarbons and water in each slice was estimated using the ideal gas law. The concentration of each chemical species was calculated based on the total concentration, total molar flow rate, and individual molar flow rate of each species (eqn (6)). These equations were used to build the rate law equations (eqn (7)–(12)) for modelling continuous PS conversion in LP-HTP. As little gas (≤2%) and char (≤2%) were observed in Experiments 1–3, the flow balance accounted only for the five species in the rate law equations (eqn (7)–(11)). The constant molar flow rate of process water (eqn (12)) was also included in the total flow rate and flow balance (eqn (4)), to model its impact on the residence time.

$$F_{\mathrm{Total}} = F_{\mathrm{StyTri}} + F_{\mathrm{StyDi}} + F_{\mathrm{StyM}} + F_{\mathrm{NonSM}} + F_{\mathrm{Poly}} + F_{\mathrm{Water}} \quad (4)$$

$$k_{\mathrm{x}} = k_{0_{\mathrm{x}}} \times \mathrm{e}^{-\frac{E_{\mathrm{a_x}}}{RT}} \quad (5)$$

$$\frac{P}{RT} = \frac{n}{V} = C_{\mathrm{Total_i}} = \frac{F_{\mathrm{Total_i}}}{\dot{V}_{\mathrm{Total_i}}} = C_{\mathrm{j_i}} \times \frac{F_{\mathrm{Total_i}}}{F_{\mathrm{j_i}}} \quad (6)$$

$$\begin{aligned}\frac{\mathrm{d}F_{\mathrm{StyTri}}}{\mathrm{d}V} &= r_{\mathrm{StyTri}} = -k_{\mathrm{T}} C_{\mathrm{StyTri_i}} \\ &= -k_{\mathrm{T}}\left(C_{\mathrm{Total_i}} \times \frac{F_{\mathrm{StyTri_i}}}{F_{\mathrm{Total_i}}}\right)\end{aligned} \quad (7)$$

$$\begin{aligned}\frac{\mathrm{d}F_{\mathrm{StyDi}}}{\mathrm{d}V} &= r_{\mathrm{StyDi}} = k_{\mathrm{T}} C_{\mathrm{StyTri}} - k_{\mathrm{D1}} C_{\mathrm{StyDi}} - k_{\mathrm{D2}} C_{\mathrm{StyDi}} \\ &= k_{\mathrm{T}}\left(C_{\mathrm{Total_i}} \times \frac{F_{\mathrm{StyTri_i}}}{F_{\mathrm{Total_i}}}\right) - k_{\mathrm{D1}}\left(C_{\mathrm{Total_i}} \times \frac{F_{\mathrm{StyDi_i}}}{F_{\mathrm{Total_i}}}\right) \\ &\quad -k_{\mathrm{D2}}\left(C_{\mathrm{Total_i}} \times \frac{F_{\mathrm{StyDi_i}}}{F_{\mathrm{Total_i}}}\right)\end{aligned} \quad (8)$$

$$\begin{aligned}\frac{\mathrm{d}F_{\mathrm{StyM}}}{\mathrm{d}V} &= r_{\mathrm{StyM}} = k_{\mathrm{T}} C_{\mathrm{StyTri}} + 2 \times k_{\mathrm{D1}} C_{\mathrm{StyDi}} - k_{\mathrm{M}} C_{\mathrm{StyM}} \\ &= k_{\mathrm{T}}\left(C_{\mathrm{Total_i}} \times \frac{F_{\mathrm{StyTri_i}}}{F_{\mathrm{Total_i}}}\right) + 2 \times k_{\mathrm{D1}}\left(C_{\mathrm{Total_i}} \times \frac{F_{\mathrm{StyDi_i}}}{F_{\mathrm{Total_i}}}\right) \\ &\quad -k_{\mathrm{M}}\left(C_{\mathrm{Total_i}} \times \frac{F_{\mathrm{StyM_i}}}{F_{\mathrm{Total_i}}}\right)\end{aligned} \quad (9)$$

$$\begin{aligned}\frac{\mathrm{d}F_{\mathrm{NonSM}}}{\mathrm{d}V} &= r_{\mathrm{NonSM}} = 2 \times k_{\mathrm{D2}} C_{\mathrm{StyDi}} + k_{\mathrm{M}} C_{\mathrm{StyM}} + 2 \times k_{\mathrm{PB}} C_{\mathrm{Poly}} - k_{\mathrm{PA}} {C_{\mathrm{NonSM}}}^2 \\ &= 2 \times k_{\mathrm{D2}}\left(C_{\mathrm{Total_i}} \times \frac{F_{\mathrm{StyDi_i}}}{F_{\mathrm{Total_i}}}\right) + k_{\mathrm{M}}\left(C_{\mathrm{Total_i}} \times \frac{F_{\mathrm{StyM_i}}}{F_{\mathrm{Total_i}}}\right) + 2 \times k_{\mathrm{PB}}\left(C_{\mathrm{Total_i}} \times \frac{F_{\mathrm{Poly_i}}}{F_{\mathrm{Total_i}}}\right) - k_{\mathrm{PA}}\left(C_{\mathrm{Total_i}} \times \frac{F_{\mathrm{NonSM_i}}}{F_{\mathrm{Total_i}}}\right)^2\end{aligned} \quad (10)$$

$$\begin{aligned}\frac{\mathrm{d}F_{\mathrm{Poly}}}{\mathrm{d}V} &= r_{\mathrm{Poly}} = -k_{\mathrm{PB}} C_{\mathrm{Poly}} + \frac{1}{2} \times k_{\mathrm{PA}} {C_{\mathrm{NonSM}}}^2 \\ &= -k_{\mathrm{PB}}\left(C_{\mathrm{Total_i}} \times \frac{F_{\mathrm{Poly_i}}}{F_{\mathrm{Total_i}}}\right) + \frac{1}{2} \times k_{\mathrm{PA}}\left(C_{\mathrm{Total_i}} \times \frac{F_{\mathrm{NonSM_i}}}{F_{\mathrm{Total_i}}}\right)^2\end{aligned} \quad (11)$$

$$\frac{\mathrm{d}F_{\mathrm{Water}}}{\mathrm{d}V} = 0 \quad (12)$$

Table 3 Estimated best-fitting intrinsic parameters for the kinetic model for continuous LP-HTP of PS

Parameter	k_0	E_a [kJ mol^{-1}]
k_T	1.8×10^{11} min^{-1}	143.9
k_{D1}	8.5×10^{7} min^{-1}	102.4
k_{D2}	1.4×10^{15} min^{-1}	205.4
k_M	1.4×10^{1} min^{-1}	28.8
k_{PA}	5.4×10^{19} mol L^{-1} min^{-1}	213.3
k_{PB}	8.2×10^{17} min^{-1}	223.1

4.2. Estimation of intrinsic parameters and standard errors for kinetic model

The intrinsic parameters were estimated by minimizing the standard errors between the observed yields in Experiments 1–3 and the model-predicted yields of the five hydrocarbon species in the kinetic model (Fig. 7). Initial estimates of the kinetic parameters (Table S9†) were obtained from the conversion data of the five species in the 28 samples of Experiments 1–3 at various T_{VA} and t_R. When determining these initial estimates, minimal conversion of the five species at 300 °C was assumed based on literature observations.[23,30] The equations and the method for finding the initial estimates are described in the ESI (eqn (S1)–(S7) and Fig. S11 and S12†).

The best-fitting parameters of k_0 and E_a for each kinetic constant (Fig. 7 and Table 3) were determined from the initial estimates by using MATLAB programs of LSQNONLIN (Non-Linear Least-Squares Fitting) and ODE45. The detailed procedure for using these optimization programs can be found in the previous batch LP-HTP study.[30] The best-fitting values of the parameters estimated from the data of Experiments 1–3 are shown in Table 3.

As shown in Fig. 8, the model-predicted yields using the best-fitting parameters agreed with the experimental data within

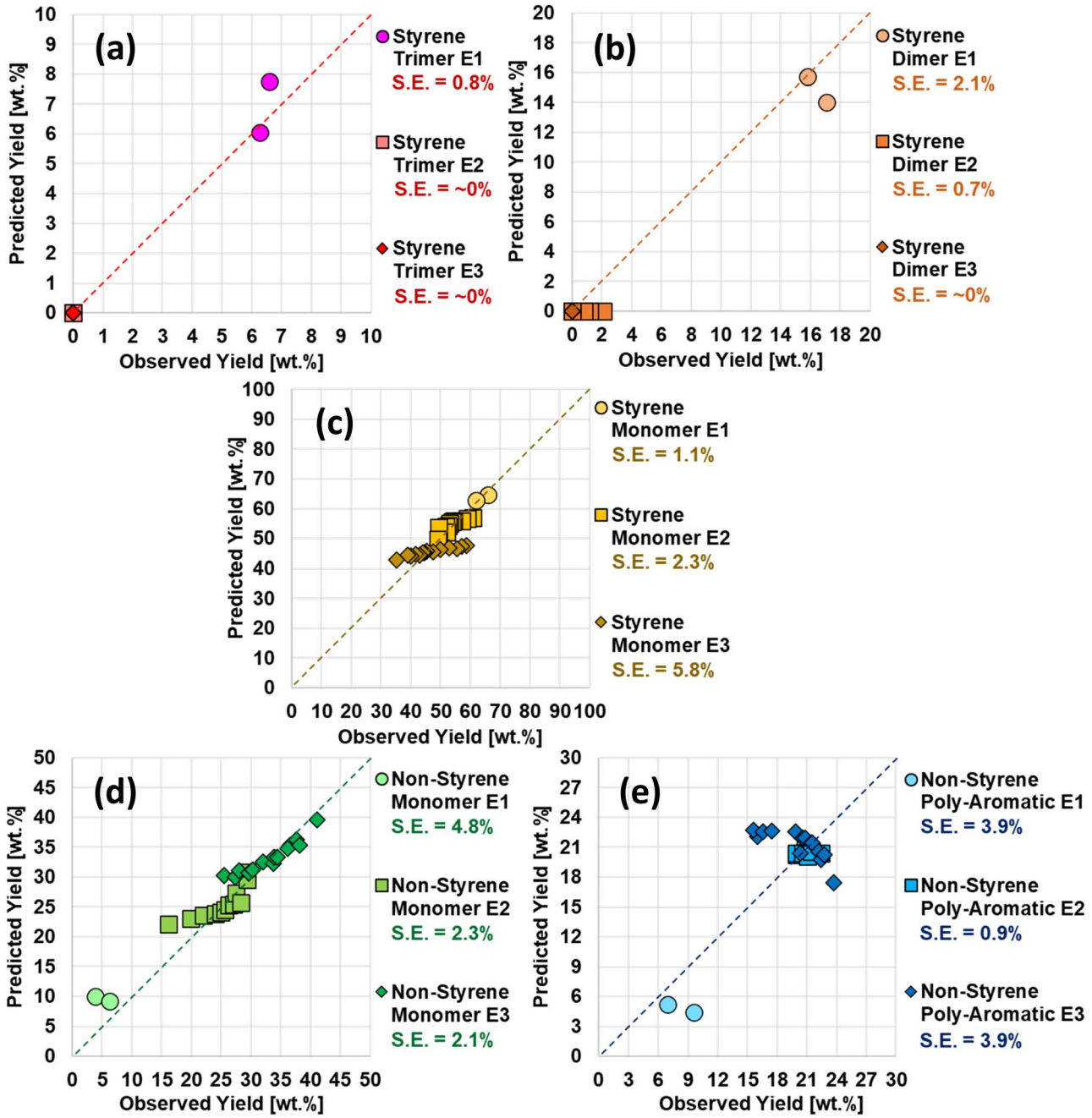

Fig. 8 Comparison of observed yields and model-predicted yields for (a) styrene trimer, (b) styrene dimer, (c) styrene monomer, (d) non-styrene monomer, and (e) non-styrene poly-aromatic produced during sample collection periods in Experiments 1–3. The standard error between model-predicted and observed yields of each species in each specific experiment is shown.

standard errors of 6%. The largest standard errors of ~6% were observed for styrene monomer (Fig. 8(c)). The model was used to obtain model-predicted yields expected for Experiment 4, which are compared with the experimental results in Section 4.3.

4.3. Testing and validation of the kinetic model with results of Experiment 4

Experiment 4 was conducted in the smaller 4.2 L Reactor B (Fig. S3(b)†), operated at slightly higher temperatures and shorter residence times, 0.7–0.8 min, than Experiment 2 (Table 2). Four oil samples were produced and analyzed. High oil yields of 96–97 wt% were observed, with yields of 3–4 wt% gas and 1 wt% char (Fig. 9(a)). As observed in Experiments 1–3, the styrene monomer yields decreased slightly with a slight increase in t_R.

Experiment 4 resulted in higher total monomer yields of 76–78 wt% compared to those of Experiment 1 (Fig. 3), as expected from the higher temperature. The styrene monomer yields, 45–52 wt%, were slightly lower than those of Experiment 2, Fig. 5(a), likely due to the slightly higher temperatures used

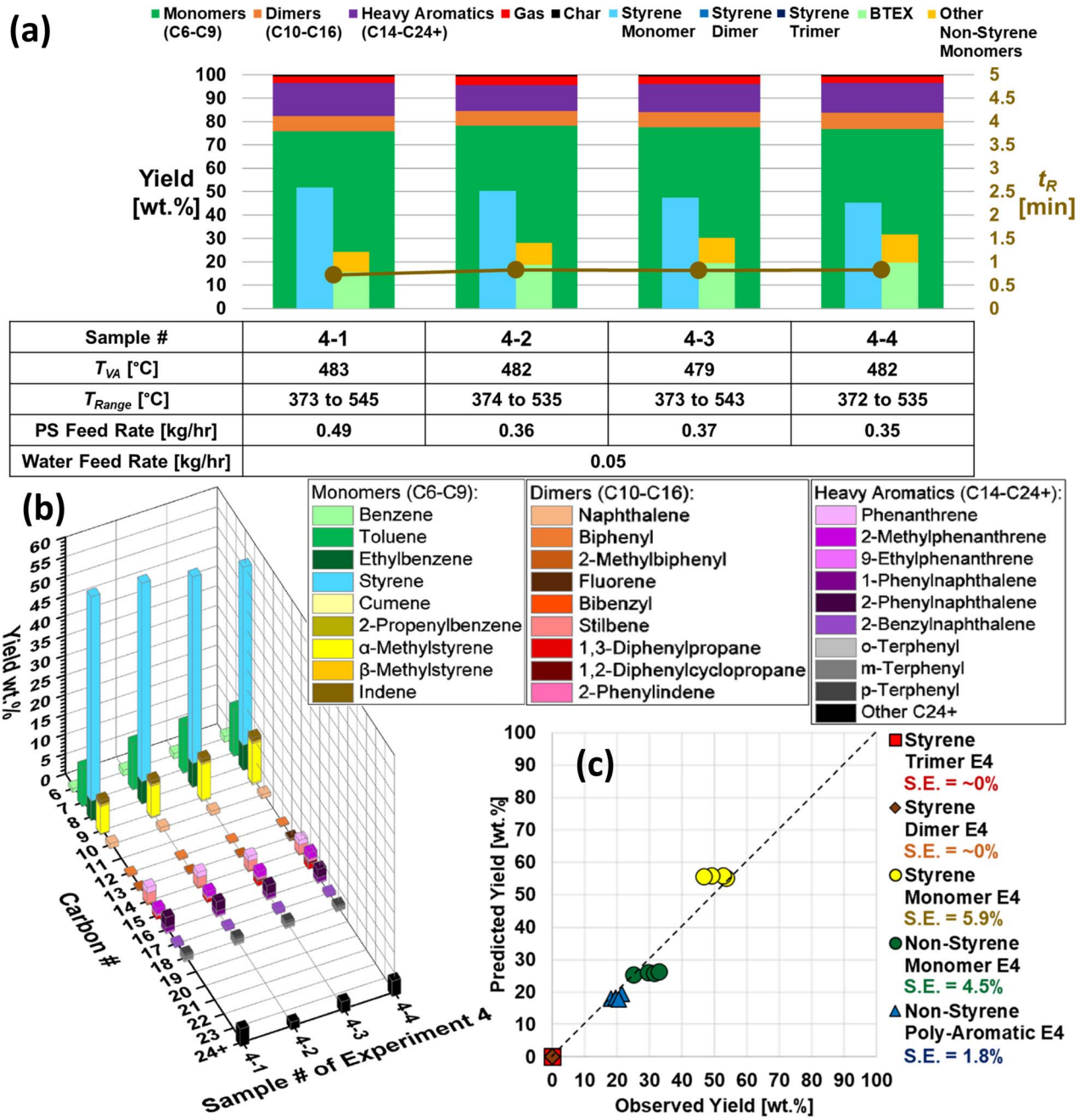

Sample #	4-1	4-2	4-3	4-4
T_{VA} [°C]	483	482	479	482
T_{Range} [°C]	373 to 545	374 to 535	373 to 543	372 to 535
PS Feed Rate [kg/hr]	0.49	0.36	0.37	0.35
Water Feed Rate [kg/hr]	0.05			

Fig. 9 (a) Yields of oil, gas, and char in sample collection periods of Experiment 4, with temperatures, residence times, feed rates, and oil compositions shown. (b) Detailed compositions of oils from Experiment 4. (c) Comparison of observed yields and model-predicted yields of chemical species produced during sample collection periods in Experiment 4, with the standard error between these yields shown for each species.

(Fig. 9(a)) The styrene monomer yields again decreased with increasing t_R, and yields of non-styrene monomers and non-styrene poly-aromatics increased (Fig. 9(b)). The trends were consistent with those in Experiments 1–3 (Fig. 4–6). The overall trends of increasing yields of non-styrene monomers and poly-aromatics with increasing t_R supported the proposed kinetic pathways (Fig. 7). Furthermore, non-styrene monomers, such as β-methylstyrene (golden rod, C_9), dimers, such as biphenyl and 2-methylbiphenyl (oranges, C_{12}–C_{13}), and heavy aromatics, such as *o*-terphenyl (light gray, C_{18}) and *p*-terphenyl (dark gray, C_{18}), were observed only in Experiment 4, with the shortest t_R of 0.7–0.8 min among all the experiments.

The temperature profiles and feed rates of PS and process water for Experiment 4 (Fig. 2(b) and Table 2) were used to independently predict the oil compositions of the 4 samples produced (Fig. 9(a–b) and Table S10†). The best-fitting parameters of the developed kinetic model (Fig. 7 and Table 3) were used to predict the oil compositions from Experiment 4 within a 6% standard error (Fig. 9(c)). The close agreement between the data and the model-predicted results of Experiment 4 supports

the kinetic model and the proposed pathways. Thus, the kinetic model is suitable for predicting oil compositions within a 6% standard error for other operating conditions. Since Experiment 4 was conducted in a smaller reactor than Experiments 1–3, the intrinsic kinetic parameters seem to be independent of the equipment used. By using this verified kinetic model, conditions for achieving higher yields of desired styrene monomers, dimers, and trimers in LP-HTP processes are identified in Section 5.

5. Application of kinetic model for product yield predictions

The kinetic model (Table 3) was used to identify the temperature and residence time for producing high yields of styrene monomers, styrene dimers, and styrene trimers in continuous LP-HTP. Simulations were conducted using various reaction temperatures (T_{VA}) and feed rates, which resulted in various

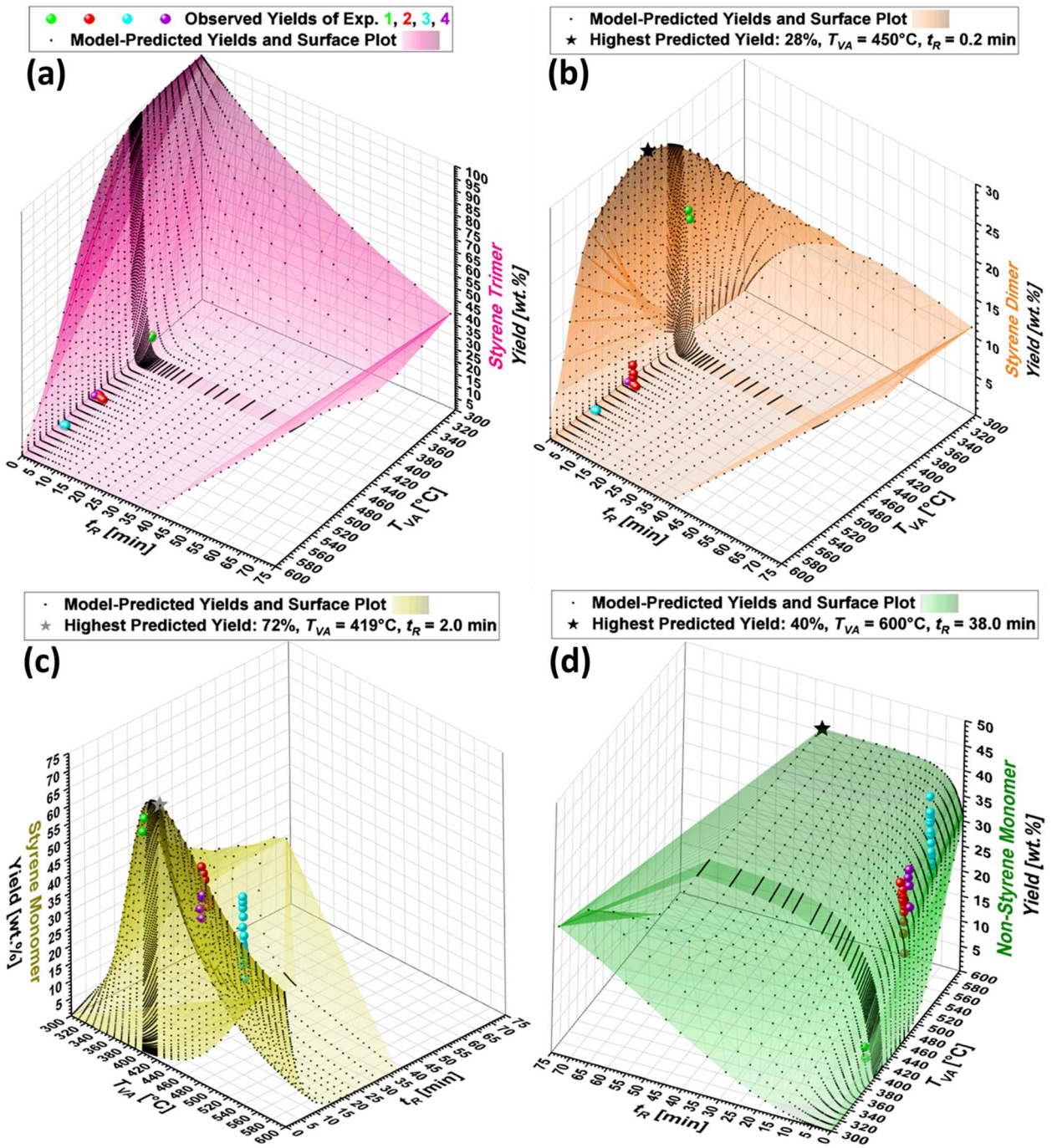

Fig. 10 *(contd.)*

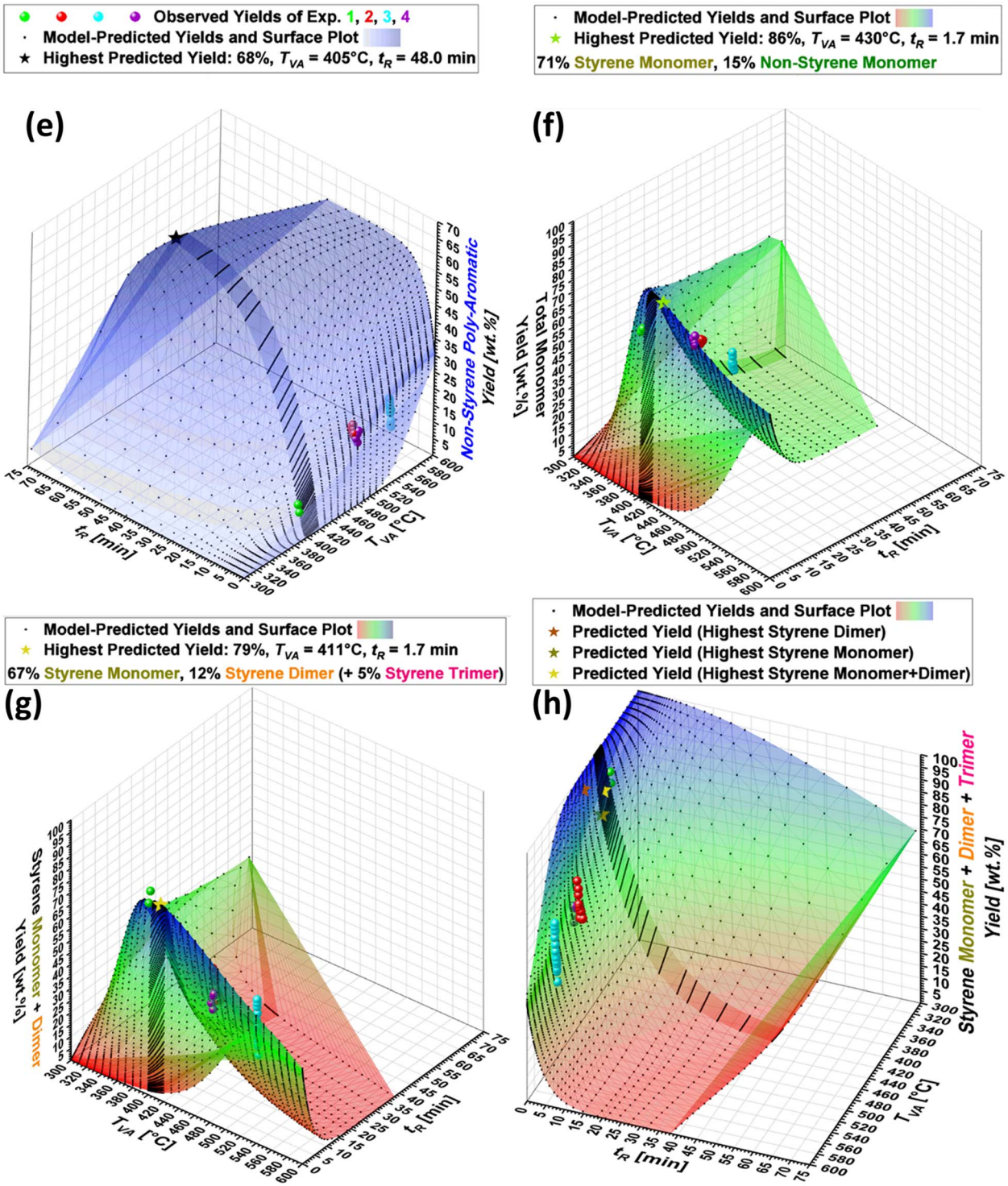

Fig. 10 Surface plots for model-predicted yields of (a) styrene trimer, (b) styrene dimer, (c) styrene monomer, (d) non-styrene monomer, (e) non-styrene poly-aromatic, (f) combined yields of styrene monomer and non-styrene monomer, (g) styrene monomer and dimer, and (h) styrene monomer, dimer, and trimer at various volume-average temperatures (T_{VA}) and residence times (t_R).

residence times (t_R). The reactor setup used in the simulations was based on the 4.2 L Reactor B (Fig. S3(b)†), with 42 volumetric slices of 0.1 L representing the reactor volume in the volumetric temperature profiles. Constant temperature profiles were used in the simulations, ranging from 300 °C to 600 °C (Fig. S13†). PS feed rates of 0.01 kg h^{-1} to 50 kg h^{-1} were used with 5 wt% water loadings, or 0.0005 kg h^{-1} to 2.5 kg h^{-1} process water feed rates. The simulated residence times ranged from 0.02 to 73.7 min at 300 °C and from 0.01 to 38.0 min at 600 °C.

Table 4 Predicted oil compositions at various volume-average temperatures (T_{VA}) and residence times (t_R)

Prediction point	T_{VA} [°C]	t_R [min]	Styrene trimer [wt%]	Styrene dimer [wt%]	Styrene monomer [wt%]	Styrene monomer + dimer [wt%]	Styrene monomer + dimer + trimer [wt%]	Non-styrene monomer [wt%]	Non-styrene poly-aromatic [wt%]	Total [wt%]
★ Highest styrene monomer	419	2.0	1	4	72	76	77	14	10	100
★ Highest styrene dimer	450	0.2	32	**28**	34	61	**93**	5	2	100
★ Highest styrene monomer + dimer	411	1.7	5	12	67	**79**	85	10	5	100

Surface plots were generated based on the kinetic model predictions to show the effects of temperature (T_{VA}) and residence time (t_R) on the simulated yields (Fig. 10). The styrene trimer yield was predicted to decrease with increasing T_{VA} or t_R (Fig. 10(a)). This result is consistent with the data from Experiments 1–4. As shown in the dark band with high-density simulation points at T_{VA} of 400–420 °C, the trimer yields decreased sharply with increasing residence times.

The styrene dimer was the intermediate species between the styrene trimer and the styrene and non-styrene monomers. The highest predicted yield of this intermediate species was 28% (±6%) at 450 °C and 0.2 min (Fig. 10(b)). The maximum yield predicted for the styrene monomer was 72% (±6%) at 419 °C and 2.0 min (Fig. 10(c)). The peak yield was due to the competing reaction for converting the styrene dimer to two non-styrene monomers, and due to the conversion of styrene monomer to non-styrene monomer (Fig. 7).

The predicted yields of the non-styrene monomer increased with increasing T_{VA} and t_R, as observed in the experiments (Fig. 10(d)). Like the previous batch LP-HTP study,[30] the reversible reaction equilibrium resulted in increased non-styrene monomer yields at higher temperatures and long residence times. At 600 °C and 38.0 min, the PS was converted to 40% non-styrene monomers and 60% non-styrene poly-aromatics. The highest non-styrene poly-aromatic yield of 68% was predicted at a lower temperature of 405 °C and 48.0 min (Fig. 10(e)), with ~31% non-styrene monomer and ~2% styrene monomer. These high residence times were reached with the lowest PS feed rate (10 g h^{-1}) used in the simulations. To reduce the yields of these non-styrene species to ≤5% each, it was predicted that lower temperatures and shorter residence times (T_{VA} < 500 °C, t_R < 1 min) should be used.

As in the batch LP-HTP study,[30] if the total concentration of hydrocarbons in the reactor decreases, the reversible reaction equilibrium in Fig. 7 shifts to the increased production of non-styrene monomers. In continuous LP-HTP, if the water loading is increased to above 5 wt%, then the total concentration decreases and the reversible reaction equilibrium shifts, resulting in higher non-styrene monomer yields. This strategy, however, would decrease the residence time and increase the amount of energy required for conversion.

Model simulations were used to identify conditions for achieving high yields of valuable chemical species (Table 4). The highest styrene monomer yield of 72% (±6%) was predicted at T_{VA} of 419 °C and t_R of 2.0 min (Fig. 10(c)). These conditions would also give a combined yield of styrene monomer, dimer, and trimer of 77%. The results of Experiment 1 at 397 °C and 2.0 min showed a styrene monomer yield of 65 wt%, slightly lower than 72%, but the combined yield of styrene monomer, dimer, and trimer was 88 wt%. Both processing conditions offer promising results.

The highest combined styrene and non-styrene monomer yields of 86% were predicted at 430 °C and 1.7 min (Fig. 10(f)). The results indicate that lower temperatures favor the conversion of styrene dimers to styrene monomers instead of non-styrene monomers. Consistent with these observations, the highest combined styrene monomer and dimer yields of 79% were predicted at 411 °C and 1.7 min (Fig. 10(g)). Furthermore, a high combined yield of 93% styrene monomer, dimer, and trimer was predicted at conditions of 450 °C and 0.2 min, which also had the highest styrene dimer yield of 28% (Fig. 10(h) and Table 4). These conditions, however, would result in styrene monomer yields lower than 72%.

The results in Table 4 suggest that a multi-stage LP-HTP process has the potential to achieve styrene monomer yields higher than 72%. The first reactor should operate at a low temperature and a short residence time to convert PS mostly to styrene trimer, dimer, and monomer, while reducing the formation of non-styrene compounds. The products from the first reactor can be separated in a distillation process into fractions of styrene monomer and combined styrene dimer and trimer. The styrene dimers and trimers would be converted in a second reactor to further increase styrene monomer yields. This multi-stage LP-HTP process has the potential to achieve high styrene monomer yields with minimal char and gas formation.

This study is focused on the conversion of virgin PS in continuous LP-HTP. Future research is needed to test the treatment of post-consumer PS waste. The reactors in this study were designed such that any non-converting

compounds, specifically inorganic fillers (such as titanium oxide or calcium carbonate), would accumulate in the solid collector at the bottom of the reactor section for ease of subsequent cleaning. Post-consumer PS waste also has other compounds, such as rubbers, flame retardants, or other polymers, which may be partially converted at the processing temperatures for PS conversion, impacting the oil yields and oil compositions. Future studies are needed to investigate how these compounds affect the performance of continuous LP-HTP processes.

6. Conclusions

Polystyrene (PS) waste is generated at a rate of 28 million tons annually, yet less than 1% is recycled. Existing methods, such as mechanical recycling, incineration, and pyrolysis, are insufficient to address the growing problem. This study presents a novel, catalyst-free, continuous low-pressure hydrothermal processing (LP-HTP) method that converts PS into valuable oils with up to 99 wt% yield and minimal char formation (<1 wt%).

Operated at atmospheric pressure (0.1 MPa), the continuous LP-HTP process is simpler and more cost-effective than batch systems, which operate at higher pressures of 2–3 MPa, or supercritical water liquefaction at over 22 MPa. Two mini-pilot LP-HTP reactors were built and tested, showing that lower temperatures and shorter residence times favored the production of styrene monomer, dimer, and trimer. Yields up to 88 wt% of styrene monomer, dimer, and trimer were achieved at 397 °C and 2.0 minutes, with styrene monomer yield of 65 wt%, while increasing temperatures and residence times increased non-styrene monomer and poly-aromatic yields.

A kinetic model was developed based on proposed reaction pathways and five major hydrocarbon product categories. The intrinsic parameters of the model were estimated from the oil compositions of the 28 samples from three experiments obtained with various temperatures and residence times. The model parameters were further verified with independent data obtained from a fourth experiment conducted in a smaller reactor. The model accurately predicted the product yields within a 6% standard error.

The verified model with the temperature- and equipment-independent parameters was then used to show how the reaction temperature and residence time affect the oil composition. Conditions of 419 °C and 2.0 minutes were identified for maximizing styrene monomer yield (72%). Different conditions of 450 °C and 0.2 minutes were also identified for predicting a high combined yield (93%) of styrene monomer, dimer, and trimer. The results demonstrated the utility of the model in process optimization and potential scalability.

If the method is further tested with PS waste and scaled up, it could be used to convert over 90% of the PS waste into valuable feedstocks, such as styrene monomer, dimer, and trimer. This technology offers a solution for PS waste management and supports the transition to a sustainable circular hydrocarbon economy.

Abbreviation

Glossary

BTEX	Benzene, toluene, ethylbenzene, and xylenes
CHP	Combined heat and power
LP-HTP	Low-pressure hydrothermal processing
LQSNONLIN	Non-linear least-squares fitting
MATLAB	Programming platform used for developing kinetic model and determining best-fitting intrinsic parameters
ODE45	Ordinary differential equation solver
PAHs	Polycyclic aromatic hydrocarbons
PS	Polystyrene
RPM	Rotations per minute
StyTri	Styrene trimer ($C_{24}H_{24}$)
StyDi	Styrene dimer ($C_{16}H_{16}$)
StyM	Styrene monomer (C_8H_8)
NonSM	Non-styrene monomer (C_6–C_9)
Poly	Non-styrene poly-aromatic (C_{10}–C_{24+})

Variables

T_{VA} [°C]	Volumetric average temperature
t_R [min]	Residence time
T [°C, K]	Temperature
P [MPa]	Pressure
n [mol]	Moles
V [L]	Volume
$V_{Reactor}$ [L]	Reaction volume
R [kJ K^{-1} mol^{-1}]	Molar constant, 8.3145 × 10^{-3} kJ K^{-1} mol^{-1}
$m_{PS_{Converted_y}}$ and $m_{PS_{Converted_{Total}}}$ [kg]	Mass of PS converted in specific sample collection period (y) of an experiment, and total mass of PS conversion in an experiment (Total)
m_{j_y} and $m_{j_{Total}}$ [kg]	Mass of product j produced in specific sample collection period (y) of an experiment, and total mass of product produced in an experiment (Total)
$\dot{V}_{AvgGasFlow_y}$ [L min^{-1}]	Average volumetric flow rate of gas during specific sample collection period (y)
t_y [min]	Length of time for specific sample collection period (y), 30 minutes
$\rho_{C_2H_6}$ 25 °C [kg L^{-1}]	Atmospheric density of ethane (C_2H_6) at 25 °C
$F_{PS_{Converted_y}}$ [molmin^{-1}]	Average molar flow rate of PS fed into reactor in specific sample collection period (y)
F_{j_i} and F_{j_f} [mol min^{-1}]	Initial and final molar flow rates of product j during conversion in reactor

F_{Total_i} and F_{Total_f} [mol min^{-1}]	Total initial and final molar flow rates during conversion in reactor
C_{j_i} and C_{j_f} [mol L^{-1}]	Initial and final molar concentrations of product j during conversion in reactor
C_{Total_i} and C_{Total_f} [mol L^{-1}]	Total initial and final molar concentrations during conversion in reactor
$\dot{V}_{j_i}$ and $\dot{V}_{j_f}$ [L min^{-1}]	Initial and final volumetric flow rates of product j during conversion in reactor
$\dot{V}_{\text{Total}_i}$ and $\dot{V}_{\text{Total}_f}$ [L min^{-1}]	Total initial and final volumetric flow rates during conversion in reactor
k_T, k_{D1}, k_{D2}, k_M and k_{PB} [min^{-1}]	First-order decomposition reaction rate constants
k_{0_T}, $k_{0_{D1}}$, $k_{0_{D2}}$, k_{0_M}, and $k_{0_{PB}}$ [min^{-1}]	Pre-exponential factors of first-order decomposition reaction rate constants
k_{PA} [L mol^{-1} min^{-1}]	Second-order combination reaction rate constant
k_{0PA} [L mol^{-1} min^{-1}]	Pre-exponential factor of second-order combination reaction rate constant
E_{aT}, E_{aD_1}, E_{aD_2}, E_{aM}, E_{aPA}, and E_{aPB} [kJ mol^{-1}]	Activation energies of reactions
j	Product of conversion, including styrene trimer, styrene dimer, styrene monomer, non-styrene monomer, and non-styrene poly-aromatic
x	Reaction in kinetic model, including T, D1, D2, M, PA, and PB
y	Identity of sample collection period during specific experiment

Data availability

The data supporting this article have been included as part of the Supplementary Information.†

Author contributions

Clayton Clarkson Gentilcore: Conceptualization, data curation, formal analysis, investigation, methodology, validation, visualization, writing – original draft, writing – review & editing. Cagri Un: Conceptualization, data curation, formal analysis, investigation, methodology, validation, visualization, writing – original draft, writing – review & editing. Josue Martinez-Maldonado: Data curation, formal analysis, methodology, validation, visualization, writing – original draft, writing – review & editing. Petr Vozka: Data curation, formal analysis, funding acquisition, investigation, methodology, supervision, validation, visualization, writing – original draft, writing – review & editing. Nien-Hwa Linda Wang: Conceptualization, formal analysis, funding acquisition, investigation, methodology, project administration, resources, supervision, visualization, writing – original draft, writing – review & editing.

Conflicts of interest

There are no conflicts to declare.

Acknowledgements

We thank Evan Sowinski of Purdue University for his help in obtaining the GC-FID data for gas compositions. We also thank Jeffrey Lynch and the staff of Research Machining Services at Purdue University for their help in the welding and fabrication of components for the mini-pilot units. This study was partially supported by the Norman and Jane Li Professorship Endowment of the Davidson School of Chemical Engineering at Purdue University, and a generous gift from Mr and Mrs Bill Smith. This study was partially supported by the National Science Foundation with an NSF HRD-2112554 grant. Clayton Clarkson Gentilcore was supported by the Norman and Jane Li Endowment of the Davidson School of Chemical Engineering at Purdue University. Cagri Un was supported by the Scientific and Technological Council of Türkiye 2219-Post-Doctoral-Research Fellowship Program. Josue Martinez-Maldonado is the recipient of a CREST fellowship, for which we are grateful. Petr Vozka was partially supported by the National Science Foundation with the NSF HRD-2112554 grant.

References

1 L. K. Ncube, A. U. Ude, E. N. Ogunmuyiwa, R. Zulkifli and I. N. Beas, An overview of plastic waste generation and management in food packaging industries, *Recycling*, 2021, **6**(1), 12.
2 United Nations Environment Programme. *From Pollution to Solution: A Global Assessment of Marine Litter and Plastic Pollution*. Nairobi, 2021.
3 R. Geyer Production, use, and fate of synthetic polymers. in *Plastic Waste and Recycling*, Academic Press, 2020, pp. 13–32.
4 S. Gündoğdu, A. Bour, A. R. Köşker, B. A. Walther, D. Napierska, F. C. Mihai and T. R. Walker, Review of microplastics and chemical risk posed by plastic packaging on the marine environment to inform the Global Plastics Treaty, *Sci. Total Environ.*, 2024, **946**, 174000.
5 C. R. de Bruin, E. de Rijke, A. P. van Wezel and A. Astefanei, Methodologies to characterize, identify and quantify nano- and sub-micron sized plastics in relevant media for human exposure: a critical review, *Environ. Sci.:Adv.*, 2022, **1**(3), 238–258.
6 J. C. Capricho, K. Prasad, N. Hameed, M. Nikzad and N. Salim, Upcycling polystyrene, *Polymers*, 2022, **14**(22), 5010.
7 N. Chaukura, W. Gwenzi, T. Bunhu, D. T. Ruziwa and I. Pumure, Potential uses and value-added products derived from waste polystyrene in developing countries: A review, *Resour., Conserv. Recycl.*, 2016, **107**, 157–165.

8 H. Li, H. A. Aguirre-Villegas, R. D. Allen, X. Bai, C. H. Benson, G. T. Beckham and G. W. Huber, Expanding plastics recycling technologies: chemical aspects, technology status and challenges, *Green Chem.*, 2022, **24**(23), 8899–9002.

9 *Recycling Today, 2019, Polystyrene recycling programs expand despite bans*, https://www.recyclingtoday.com/news/polystyrene-recycling-programs-expand-despite-bans/.

10 J. A. Conesa, Adsorption of PAHs and PCDD/Fs in microplastics: a review, *Microplastics*, 2022, **1**(3), 346–358.

11 D. Choi, J. Bang, T. Kim, Y. Oh, Y. Hwang and J. Hong, In vitro chemical and physical toxicities of polystyrene microfragments in human-derived cells, *J. Hazard. Mater.*, 2020, **400**, 123308.

12 X. Zhao, M. Korey, K. Li, K. Copenhaver, H. Tekinalp, S. Celik and S. Ozcan, Plastic waste upcycling toward a circular economy, *Chem. Eng. J.*, 2022, **428**, 131928.

13 Z. O. Schyns and M. P. Shaver, Mechanical recycling of packaging plastics: A review, *Macromol. Rapid Commun.*, 2021, **42**(3), 2000415.

14 K. Ragaert, L. Delva and K. Van Geem, Mechanical and chemical recycling of solid plastic waste, *J. Waste Manage.*, 2017, **69**, 24–58.

15 L. K. Ncube, A. U. Ude, E. N. Ogunmuyiwa, R. Zulkifli and I. N. Beas, An overview of plastic waste generation and management in food packaging industries, *Recycling*, 2021, **6**(1), 12.

16 O. Eriksson and G. Finnveden, Plastic waste as a fuel-CO 2-neutral or not?, *Energy Environ. Sci.*, 2009, **2**(9), 907–914.

17 S. M. Al-Salem, Energy production from plastic solid waste (PSW), in *Plastics to Energy*, William Andrew Publishing, 2019, pp. 45–64.

18 A. Vlasopoulos, J. Malinauskaite, A. Żabnieńska-Góra and H. Jouhara, Life cycle assessment of plastic waste and energy recovery, *Energy*, 2023, **277**, 127576.

19 R. Verma, K. S. Vinoda, M. Papireddy and A. N. S. Gowda, Toxic pollutants from plastic waste-a review, *Procedia Environ. Sci.*, 2016, **35**, 701–708.

20 K. Sun, Y. Song, F. He, M. Jing, J. Tang and R. Liu, A review of human and animals exposure to polycyclic aromatic hydrocarbons: Health risk and adverse effects, photo-induced toxicity and regulating effect of microplastics, *Sci. Total Environ.*, 2021, **773**, 145403.

21 I. M. Maafa, Pyrolysis of polystyrene waste: A review, *Polymers*, 2021, **13**(2), 225.

22 M. Artetxe, G. Lopez, M. Amutio, I. Barbarias, A. Arregi, R. Aguado and M. Olazar, Styrene recovery from polystyrene by flash pyrolysis in a conical spouted bed reactor, *J. Waste Manage.*, 2015, **45**, 126–133.

23 K. B. Park, Y. S. Jeong, B. Guzelciftci and J. S. Kim, Two-stage pyrolysis of polystyrene: Pyrolysis oil as a source of fuels or benzene, toluene, ethylbenzene, and xylenes, *Appl. Energy*, 2020, **259**, 114240.

24 A. Zayoud, H. D. Thi, M. Kusenberg, A. Eschenbacher, U. Kresovic, N. Alderweireldt and K. M. Van Geem, Pyrolysis of end-of-life polystyrene in a pilot-scale reactor: Maximizing styrene production, *Waste Manage.*, 2022, **139**, 85–95.

25 B. Joshi, H. Raghav, A. Agrawal, B. P. Vempatapu, A. Ray and B. Sarkar, Sustainable production of styrene from catalytic recycling of polystyrene over potassium promoted Fe–Al 2 O 3 catalyst, *Sustainable Energy Fuels*, 2023, **7**(5), 1256–1264.

26 J. S. Kim, W. Y. Lee, S. B. Lee, S. B. Kim and M. J. Choi, Degradation of polystyrene waste over base promoted Fe catalysts, *Catal. Today*, 2003, **87**(1–4), 59–68.

27 V. Daligaux, R. Richard and M. H. Manero, Deactivation and regeneration of zeolite catalysts used in pyrolysis of plastic wastes—a process and analytical review, *Catalysts*, 2021, **11**(7), 770.

28 M. Kusenberg, M. Roosen, A. Zayoud, M. R. Djokic, H. D. Thi, S. De Meester and K. M. Van Geem, Assessing the feasibility of chemical recycling *via* steam cracking of untreated plastic waste pyrolysis oils: Feedstock impurities, product yields and coke formation, *J. Waste Manage.*, 2022, **141**, 104–114.

29 M. Bernardo, N. Lapa, M. Gonçalves, R. Barbosa, B. Mendes, F. Pinto and I. Gulyurtlu, Toxicity of char residues produced in the co-pyrolysis of different wastes, *Waste Manage.*, 2010, **30**(4), 628–635.

30 C. Gentilcore, K. Jin, G. Barzallo, P. Vozka and N. H. L. Wang, Low-pressure hydrothermal processing for conversion of polystyrene into oils, *J. Environ. Chem. Eng.*, 2024, **12**(5), 113836.

31 C. Un, C. Gentilcore, K. Ault, H. Gieng, P. Vozka and N. H. L. Wang, Low-Pressure Hydrothermal Processing of Disposable Face Masks into Oils, *Processes*, 2023, **11**(10), 2819.

32 K. Jin, P. Vozka, C. Gentilcore, G. Kilaz and N. H. L. Wang, Low-pressure hydrothermal processing of mixed polyolefin wastes into clean fuels, *Fuel*, 2021, **294**, 120505.

33 J. Nisar, G. Ali, A. Shah, M. Iqbal, R. A. Khan, F. Anwar and M. S. Akhter, Fuel production from waste polystyrene *via* pyrolysis: Kinetics and products distribution, *J. Waste Manage.*, 2019, **88**, 236–247.

34 R. W. J. Westerhout, J. Waanders, J. A. M. Kuipers and W. P. M. van Swaaij, Kinetics of the low-temperature pyrolysis of polyethene, polypropene, and polystyrene modeling, experimental determination, and comparison with literature models and data, *Ind. Eng. Chem. Res.*, 1997, **36**(6), 1955–1964.

35 G. P. Ravanetti and M. Zini, A study on the thermal degradation kinetics of syndiotactic polystyrene by thermogravimetric analysis, *Thermochim. Acta*, 1992, **207**, 53–64.

36 H. Nishizaki, K. Yoshida and J. H. Wang, Comparative study of various methods for thermogravimetric analysis of polystyrene degradation, *J. Appl. Polym. Sci.*, 1980, **25**(12), 2869–2877.

37 T. Bremner, A. Rudin and D. G. Cook, Melt flow index values and molecular weight distributions of commercial thermoplastics, *J. Appl. Polym. Sci.*, 1990, **41**(7-8), 1617–1627.

38 K. Copenhaver, T. Smith, K. Armstrong, D. Kamath, M. Rencheck, S. Bhagia and S. Ozcan, Recyclability of additively manufactured bio-based composites, *Composites, Part B*, 2023, **255**, 110617.

39 National Institute of Standards and Technology (NIST). *NIST Chemistry WebBook, SRD 69*, Thermophysical Properties of Fluid Systems, 2018, **https://webbook.nist.gov/chemistry/fluid/**.
40 ASTM D86-23ae2, *Standard Test Method for Distillation of Petroleum Products and Liquid Fuels at Atmospheric Pressure*, ASTM International, West Conshohocken, PA, 2024, **https://www.astm.org**.
41 P. Vozka and G. Kilaz, How to obtain a detailed chemical composition for middle distillates *via* GC× GC-FID without the need of GC× GC-TOF/MS, *Fuel*, 2019, **247**, 368–377.
42 L. Šindelářová, E. N. Luu and P. Vozka, Comparison of gas and kerosene oils chemical composition before and after hydrotreating using comprehensive two-dimensional gas chromatography, *J. Chromatogr. Open*, 2022, **2**, 100068.
43 J. Zhou, Y. Qiao, W. Wang, E. Leng, J. Huang, Y. Yu and M. Xu, Formation of styrene monomer, dimer and trimer in the primary volatiles produced from polystyrene pyrolysis in a wire-mesh reactor, *Fuel*, 2016, **182**, 333–339.
44 B. N. Jang and C. A. Wilkie, The thermal degradation of polystyrene nanocomposite, *Polymer*, 2005, **46**(9), 2933–2942.
45 T. M. Kruse, O. S. Woo, H. W. Wong, S. S. Khan and L. J. Broadbelt, Mechanistic modeling of polymer degradation: a comprehensive study of polystyrene, *Macromolecules*, 2002, **35**(20), 7830–7844.
46 J. Wang, Y. Ma, S. Li and C. Yue, Catalytic pyrolysis of polystyrene in different reactors: Effects of operating conditions on distribution and composition of products, *J. Anal. Appl. Pyrolysis*, 2024, **177**, 106366.
47 J. Huang, X. Li, H. Meng, H. Tong, X. Cai and J. Liu, Studies on pyrolysis mechanisms of syndiotactic polystyrene using DFT method, *Chem. Phys. Lett.*, 2020, **747**, 137334.
48 T. Lee, S. Jung, Y. K. Park, T. Kim, H. Wang, D. H. Moon and E. E. Kwon, Catalytic pyrolysis of polystyrene over steel slag under CO2 environment, *J. Hazard. Mater.*, 2020, **395**, 122576.